UNIVERSITY OF OKLAHOMA

GRADUATE COLLEGE

MAGNETOSTRATIGRAPHY OF CENOZOIC SEDIMENTS IN THE BIDAHOCHI FORMATION AND THE LOWER COLORADO RIVER CORRIDOR

A THESIS

SUBMITTED TO THE GRADUATE FACULTY

in partial fulfillment of the requirements for the

Degree of

MASTER OF SCIENCE

By

JOSEPH REDMAN MORRELL

Norman, Oklahoma

2025

Downloaded from SHAREOK. Persistent Handle URL: https://hdl.handle.net/11244/341676

MAGNETOSTRATIGRAPHY OF CENOZOIC SEDIMENTS IN THE BIDAHOCHI FORMATION AND THE LOWER COLORADO RIVER CORRIDOR

A THESIS APPROVED FOR THE

SCHOOL OF GEOSCIENCES

BY THE COMMITTEE CONSISTING OF

Dr. Shannon Dulin, Chair

Dr. Gilby Jepson

Dr. Ryan Crow

© Copyright by Joseph Redman Morrell 2025

All Rights Reserved.

ACKNOWLEDGEMENTS

I want to first and foremost thank God and my family for always supporting me in this journey of my masters. I want to thank my late father and grandfather for inspiring me to pursue a career within the energy industry.

I want to thank my roommate and longtime friend Jarah Burdette for always helping through my undergraduate and graduate years here at the University of Oklahoma. I also want to thank Shannon Dulin for inspiring me to switch over from Petroleum Engineering to Petroleum Geology while I was an undergraduate. I will never forget the fun times we spent together whether that was out in the field, in the classroom, or in our offices. I am truly grateful Shannon!

I want to thank everyone that was on my committee including Ryan Crow, Sarah George, and Gilby Jepson. I also want to thank Michael Petronis at the University of New Mexico Highlands for letting me use his paleomagnetism lab. To everyone else that has helped me in this journey, I am forever grateful.

Any person(s) wishing to conduct geological investigations on the Navajo Nation must first apply for, and receive a permit from the Minerals Department, P.O. Box 1910, Window Rock, Arizona 86515 and telephone no. (928) 871-6587.

Table of Contents

ACKNOWLEDGEMENTS iv
FIGURES vii
TABLES viii
ABSTRACT ix
INTRODUCTION 1
GEOLOGIC BACKGROUND 7
Bidahochi Formation 9
Previous Geochronological Studies (Bidahochi) 9
Bouse Formation 11
Previous Geochronological Studies (Bouse) 12
METHODS 16
Field Sampling 16
Sample Preparation 17
Rock Magnetic Study 19
Curie Temperature Analysis 19
RESULTS 19
Quality Analysis (Grading) 19
Magnetostratigraphy 23
Roberts Mesa 23
Greasewood 24
Hart Mine Wash (HMW) 25
Lost Cabin Wash (LCWBC & LCWSW) 25
Rock Magnetic Analysis 35
Curie Temperature Analysis 35
DISCUSSION 39
Magnetostratigraphy 39
Roberts Mesa 39
Greasewood 40
Hart Mine Wash 41
Lost Cabin Wash 42

Curie Temperature Analysis 43
Poor Data Results 43
Sedimentation Rates 44
Big Picture 46
CONCLUSIONS 47
REFERENCES 49

FIGURES

Figure 1: A: Locations that were sampled within this study and the only magnetostratigraphic study done within the Bidahochi (White Cone). B: Overview of Roberts Mesa and sample site RM-2. C: Sampling within Greasewood canyon and sample site GW-0. 4
Figure 2: Location map showing where LCWSW and LCWBC samples are located within Cottonwood and Mohave Valleys. 6
Figure 3: Modified from (Lindsay et al., 1984). Figure of White Cone with the GPTS superimposed...11
Figure 4: Figure from Crow et al., (2021) A: summarizes the previously completed geochronological studies on the LOCO showing sampling locations and outcrops of pre- and post-Colorado River deposits. B-E: show depositional relationships, previous sampling locations, and structures within the LOCO. 15
Figure 5: Location of HMW1 – HMW3 in relation to the HMW ash. GPTS is modified from Sanger (2023). Black stars indicate a site with normal polarity inclinations and white stars indicate reverse polarity inclinations. 17
Figure 6: Representative Zijderveld [1967] diagrams and equal area projections used for this study. Closed boxes represent declination values and open boxes represent inclination values. NRM and ChRM are both labeled. A quality data shown. 20
Figure 7: Representative Zijderveld [1967] diagrams and equal area projections used for this study. Closed boxes represent declination values and open boxes represent inclination values. NRM and ChRM are both labeled. B quality data shown. 21
Figure 8: Representative Zijderveld [1967] diagrams and equal area projections used for this study. Closed boxes represent declination values and open boxes represent inclination values. NRM and ChRM are both labeled. C quality data shown. 22
Figure 9: Representative Zijderveld [1967] diagrams and equal area projections used for this study. Closed boxes represent declination values and open boxes represent inclination values. NRM and ChRM are both labeled. D quality data shown. 22
Figure 10: Representative Zijderveld [1967] diagrams and equal area projections used for this study. Closed boxes represent declination values and open boxes represent inclination values. F quality data shown. 23
Figure 11: Thermomagnetic curves displaying all the Roberts Mesa samples that were run. The y-axis represents the magnetic moment of the sample in kilo Tesla and the x-axis represents the overall temperature of the sample in degrees Celsius. 36
Figure 12: Thermomagnetic curves displaying all the Greasewood samples that were run. The y-axis represents the magnetic moment of the sample in kilo Tesla and the x-axis represents the overall temperature of the sample in degrees Celsius. 37
Figure 13: Thermomagnetic curves on the top are run by Sanger (2023) for HMW and the one on the bottom was run for this study. The y-axis represents the magnetic moment of the sample in kilo Tesla and the x-axis represents the overall temperature of the sample in 37

Figure 14: Thermomagnetic curves displaying the Lost Cabin Wash sample that was run. The y-axis represents the magnetic moment of the sample in kilo Tesla and the x-axis represents the overall temperature of the sample in degrees Celsius. 38
Figure 15 Stratigraphic column showing sample location in Roberts Mesa including the magnetostratigraphy (red) and the preliminary ash dates (blue). Black circles represent reverse polarity samples and black circles represent normal polarity samples. The green circle represents anything that was graded an A or B. Yellow circles represent anything that was graded a C and the red circles represent D graded samples. 40
Figure 16 Stratigraphic column showing sample location in Greasewood Canyon including the magnetostratigraphy (red) and the preliminary ash dates (blue). Black circles represent reverse polarity samples and black circles represent normal polarity samples. The green circle represents anything that was graded an A or B. Yellow circles represent anything that was graded a C and the red circles represent D graded samples. 41
Figure 17: Modified from Schwing (2019) shows the Bouse Fluvial incision site with black stars indicating sites that were run in this study and red stars representing samples that were taken by Schwing......43
Figure 18 Compilation of Magnetostratigraphic Data within the Bidahochi Basin & the Lower Colorado River Corridor. Red callouts represent Lindsay et al. (1984) interpretation of White Cone. Green callout represents this studies interpretation of the upper member of the Bidahochi at Roberts Mesa and Greasewood. Blue callouts represent the chrons found within the LOCO. Important ash dates are listed within the Bidahochi and the LOCO. Red bracket is representative of a reinterpretation of Sanger (2023). Black brackets are interpretations of magnetostratigraphic data done throughout the Bidahochi and the LOCO......46

TABLES

Table 1 ChRM's for Roberts Mesa (RM) location 28
Table 2 Site Mean Directions – ChRM's for Greasewood (GW) location.....32
Table 3 Site Mean Directions – ChRM's for Hart Mine Wash (HMW) location 32
Table 4 Site Mean Directions – ChRM's for Bouse Incision (LCWBC) location.....33
Table 5 Site Mean Directions – ChRM's for Lost Cabin Beds (LCWSW) location.....34

ABSTRACT

Magnetostratigraphy utilizes Earth's ancient magnetic field to help define timing of deposition and potential depositional rates of a formation, especially when coupled with other dating methods. The Bidahochi Formation, located upstream of the Grand Canyon, contains fluvial-lacustrine deposits that record the presence of paleo Hopi Lake that was filled by the early Colorado River. Previous geochronological and paleomagnetic studies place the onset of sedimentation in the Bidahochi Formation around 16 Ma and continued until approximately 5.9 Ma. Downstream of the Grand Canyon, the Bouse Formation within the lower Colorado River corridor (LOCO) records the arrival of the Colorado River to the southern drainage basins. Lost Cabin beds within Cottonwood and Mohave valleys of the LOCO were deposited prior to Colorado River integration. This study investigates sediments east of the Grand Canyon and combines new and previous data south of the Grand Canyon (LOCO) to further constrain the timing of Colorado River integration and related sediments using magnetostratigraphic sampling and analytical methods. 81 total samples were taken from two different sites within the upper member of the Bidahochi Formation to determine the magnetic polarity and correlate them to the Geomagnetic Polarity Time Scale (GPTS). Three sites with 27 samples within the LOCO were chosen to further constrain previous magnetostratigraphic work done on the Lost Cabin beds (pre Bouse) and Bouse Formation. Magnetite and titanomagnetite were identified to be the primary minerals that held magnetic remanence within the samples. All the samples from this study are interpreted to have a primary magnetization that is further interpreted as a detrital remanent magnetization (DRM), held in magnetite and/or titanomagnetite. Upper Bidahochi samples yielded majority normal polarity inclinations except for a handful of samples. The normal polarity samples within the upper Bidahochi are interpreted to be within the normal C3An.2n (6.727 Ma – 6.386 Ma) polarity subchron with the handful of reverse polarity samples interpreted to be an excursion within the C3An.2n subchron. New depositional rates within the upper Bidahochi were calculated from this data and range from 0.313 mm/yr to 0.175 mm/yr. In the LOCO, Lost Cabin bed samples bolstered previous magnetostratigraphy studies, with all reverse polarity inclinations interpreted to be within

the reverse C3r Gilbert chron (6.023 Ma – 5.235 Ma). A Bouse channel within the older Lost Cabin beds also yielded similar results from previous study, showing three reverse polarity sites and one ambiguous normal polarity site. Hart Mine Wash Bouse samples were taken above and below the ~4.8 Ma Hart Mine wash ash to try and further constrain a potential reversal at this location, but more sampling is needed.

INTRODUCTION

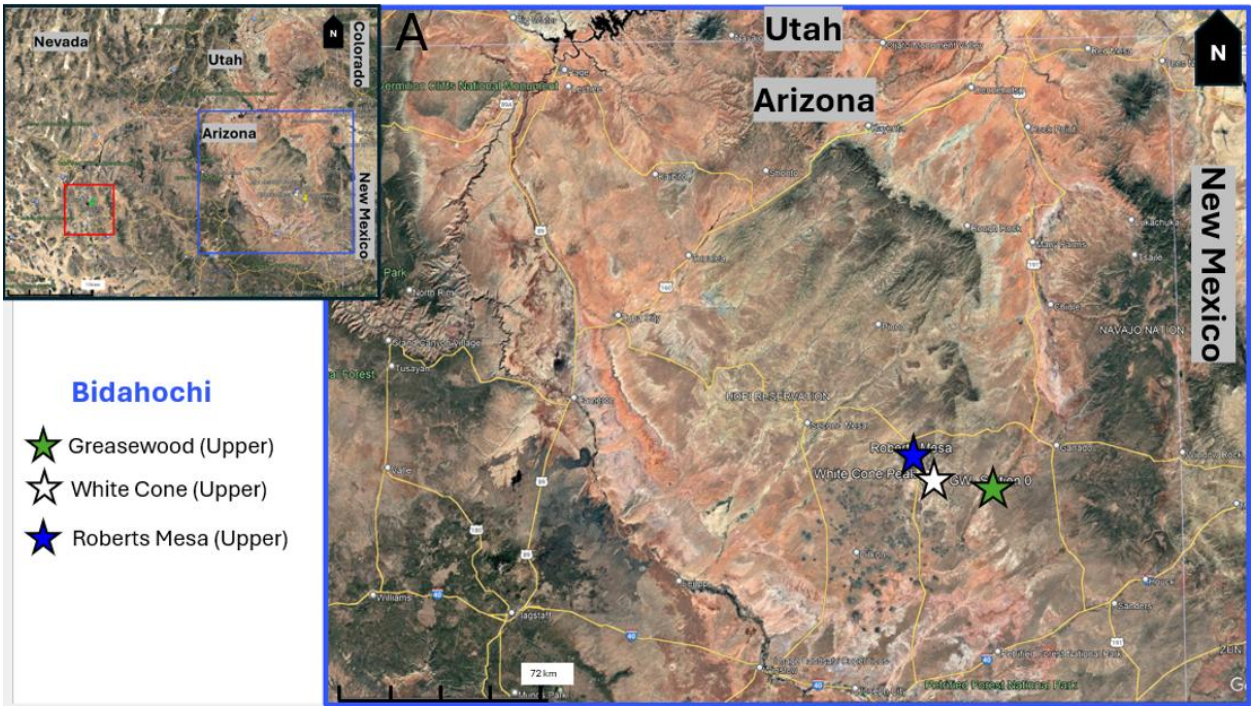
The evolution of the early Colorado River and its carving of the Grand Canyon has been disputed in the literature for over a century since John Wesley Powell first surveyed the area 150 years ago (Lucchitta, 1984, 1989, 1990; Young and Spamer, 2001; Ranney, 2005; Flowers et al., 2008; Pelletier, 2010; Wernicke, 2011; Beard et al., 2011; Douglass, 2011; Karlstrom et al., 2011, 2014). The Colorado Plateau first began uplifting between 80 and 50 Ma with continual uplift occurring today (Karlstrom et al., 2011, 2014; Roberts et al., 2012; Aslan et al., 2019). Available evidence suggests that the Colorado River first exited the Colorado Plateau sometime after ~6 Ma and reached the Gulf of California between 4.8 and 4.6 Ma (Crow et al., 2021). Rates of Colorado River incision and related Colorado Plateau exhumation during that time are debated (Tanski et al. 2025; Karlstrom et al., 2008), but generally characterized by long-term uplift and erosion. The Bidahochi Formation represents an unusual exception: the sedimentary record of a large, long-lived basin in the southeastern corner of the Plateau that formed and was filled between ~16 and 6 Ma. This study examines the upper member of the Bidahochi Formation on the Colorado Plateau using magnetostratigraphy to refine depositional ages and sedimentation rates, with the broader goal of gaining insight into the timing of integration and the development of the Colorado River. In addition, the study integrates new magnetostratigraphic and geochronological data from the Bouse Formation and Lost Cabin beds in the Lower Colorado River Corridor (LOCO) to further constrain the timing of Colorado River integration.

Upstream of the Grand Canyon and east of the Kaibab-Coconino Plateau, the upper member of the Bidahochi Formation contains fluvial-lacustrine deposits that record the presence of paleo Hopi Lake that some suggest was filled by the early Colorado River (Repenning and Irwin 1954; Douglass et al., 1999, 2020; Dallege 1999; Dickenson 2011). The topic of debate related to the Bidahochi Formation is the depositional environment and

if it formed a Colorado-River-fed lake that contributed to integration by a process such as lake spillover. Multiple arguments suggest that the lake/basin was unconstrained on the western side and therefore extended to the Kaibab Plateau. This unconstrained western boundary in the Bidahochi basin has been used as evidence that spillover is a viable mechanism for initial incision into the Grand Canyon (Repenning et al., 1958; Douglass 1999, 2020; Dallegge 1999). Alternative hypotheses argue that the upper member of the Bidahochi is not Colorado River derived and that the maximum elevations of the Bidahochi Formation are not compatible with a lake spillover model unless post Bidahochi deformation or pre Bidahochi canyon cutting/ erosion occurred (Dickenson et al., 2013). Sedimentation rates within the upper member of the Bidahochi have been inferred using magnetostratigraphy (Lindsay et al., 1984) and do not align with Colorado River sedimentation. Within this study, newly acquired magnetostratigraphic samples are used to refine timing of deposition and depositional rates within the upper member of the Bidahochi Formation with implications for its depositional environment.

Previous geochronological and paleomagnetic studies place the onset of sedimentation in the Bidahochi around 16 Ma continuing until approximately 5.9 Ma (Lindsay et al., 1984; Dallegge, 1999; Dallegge et al., 2003; Morgan and White, 2005). The lower age is derived from a biotite $^{40}Ar/^{39}Ar$ age of 15.46 ± 0.36 Ma, a modeled glass $^{40}Ar/^{39}Ar$ age of 15.8 Ma from a sample that was geochemically correlated to the 15.84 ± 0.05 Ma Echo Spring Mountain felsic ash bed (Dallegge et al., 2003). The upper age is derived from the highest paleomagnetic reversal at White Cone Peak, which is an outcrop of upper Bidahochi Formation. There is also a recently dated detrital sanidine $^{40}Ar/^{39}Ar$ maximum deposition age (MDA) age of 6.07 ± 0.07 that was found in the upper Bidahochi near Roberts Mesa (Heizler et al., 2021). The magnetostratigraphic constraints on the upper age of the White Cone section is poorly constrained because there is an additional 100+ meters of sediment within the upper member of the Bidahochi not present at White Cone but which are exposed nearby at Roberts Mesa and Greasewood Canyon (Lindsay et al., 1984; Douglass et al., 2020). The magnetostratigraphy done at White Cone by Lindsay et al. (1984) can be improved upon because magnetometers are more sensitive than they were

four decades ago. This project will use magnetostratigraphy to better constrain the timing of deposition and depositional rates within the upper member of the Bidahochi at Greasewood Canyon and Roberts Mesa—two previously unsampled locations— **(Figure 1).**



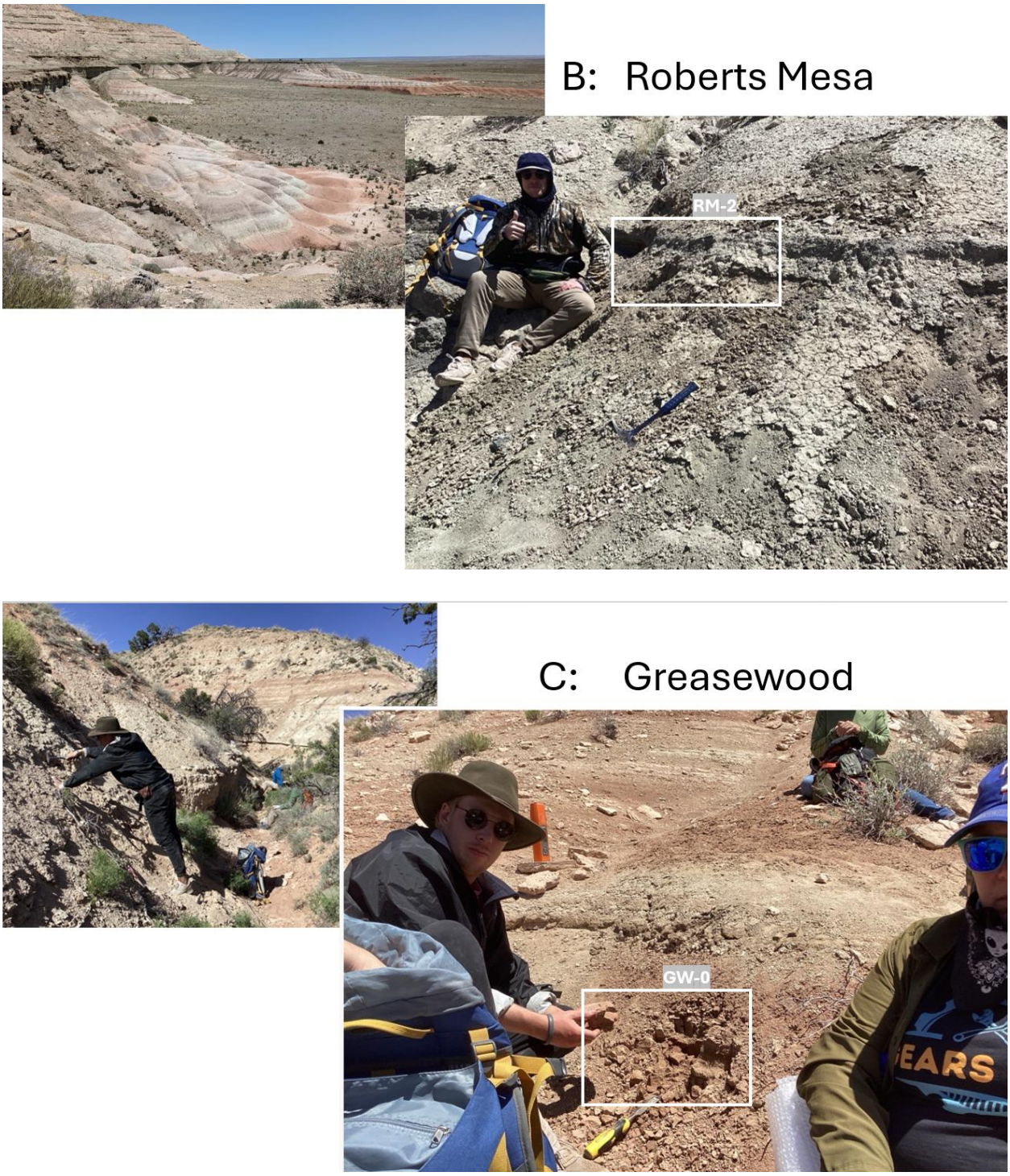


Figure 1: A: Locations that were sampled within this study and the only magnetostratigraphic study done within the Bidahochi (White Cone). B: Overview of Roberts Mesa and sample site RM-2. C: Sampling within Greasewood canyon and sample site GW-0.

The ancestral Colorado River likely followed a southwestward path similar to the current course through the Grand Canyon, before sharply veering southward past present-day Lake Mead. Downstream of the Grand Canyon, the Bouse Formation within the Lower Colorado River Valley (LOCO) records the arrival of the Colorado River to the southern drainage basins. The depositional model for the Bouse Formation in the northernmost of the LOCO drainage basins is largely agreed upon, with evidence suggesting that a series of paleo-divides separated the corridor into isolated basins/lakes (Spencer and Patchett, 1997; House et al., 2008; Roskowski et al., 2010; Pearthree and House, 2014; O'Connell et al., 2017; Bright et al., 2018; Spencer et al., 2021). As the Colorado River passed through these basins, they filled with sediment and eventually spilled over into the next closed basin, a process informally known as "fill and spill". The fill-and-spill process continued southward, first reaching Cottonwood Valley, followed by Mohave Valley, Chemehuevi Valley, and the Blythe Basin. Finally, it would have reached the Fish-Creek Vallecito Basin near the Salton Trough, which has subsequently been shifted to the northwest by movement of the San Andreas Fault Zone (Dorsey et al., 2011). The opposing depositional model for the Bouse suggests that the southernmost Blythe basin of the LOCO was a marine estuarine system where lacustrine/fluvial waters meet the sea (McDougall, 2008; McDougall and Miranda-Martinez, 2014; Dorsey and Humphreys, 2017; Miranda Martinez et al., 2017; Gardner and Dorsey, 2021). The evidence of a marine estuarine depositional system within the Blythe basin is tied to marine fossil assemblages (mostly foraminifera species), interpreted shallow sea sedimentary structures, and a high carbonate content within the Bouse marl.

The Lost Cabin beds are well preserved pre-Bouse deposits within Cottonwood Valley, the northernmost LOCO basin. Schwing (2019) conducted magnetostratigraphy on flat- lying Lost Cabin beds in Cottonwood Valley. These Miocene beds were mapped within Cottonwood Valley and were found to be stratigraphically below the Bouse marl, which suggests that these Lost Cabin beds pre-date the inception of the Colorado River (Schwing., 2019; Crow et al., 2019). A geomagnetic polarity reversal was captured within these Lost Cabin Wash beds in Cottonwood Valley and tied to the C3r to C3n.4n (Thvera)

subchron transition due to the presence of a 5.35 Ma ash below the reversal (Schwing., 2019; Crow et al., 2021). This documented reversal acts as the maximum age of arrival of the Colorado River to the basin.

Schwing (2019) collected samples within Cottonwood Valley from channels cut in the Lost Cabin bed that were filled with Bouse deposits. In this project, magnetostratigraphy will be performed on samples from these sites not analyzed by Schwing to determine if further constraint the timing of Bouse Formation deposition within Cottonwood Valley is possible. Two sites are considered within Cottonwood Valley and are shown within **Figure 2.**

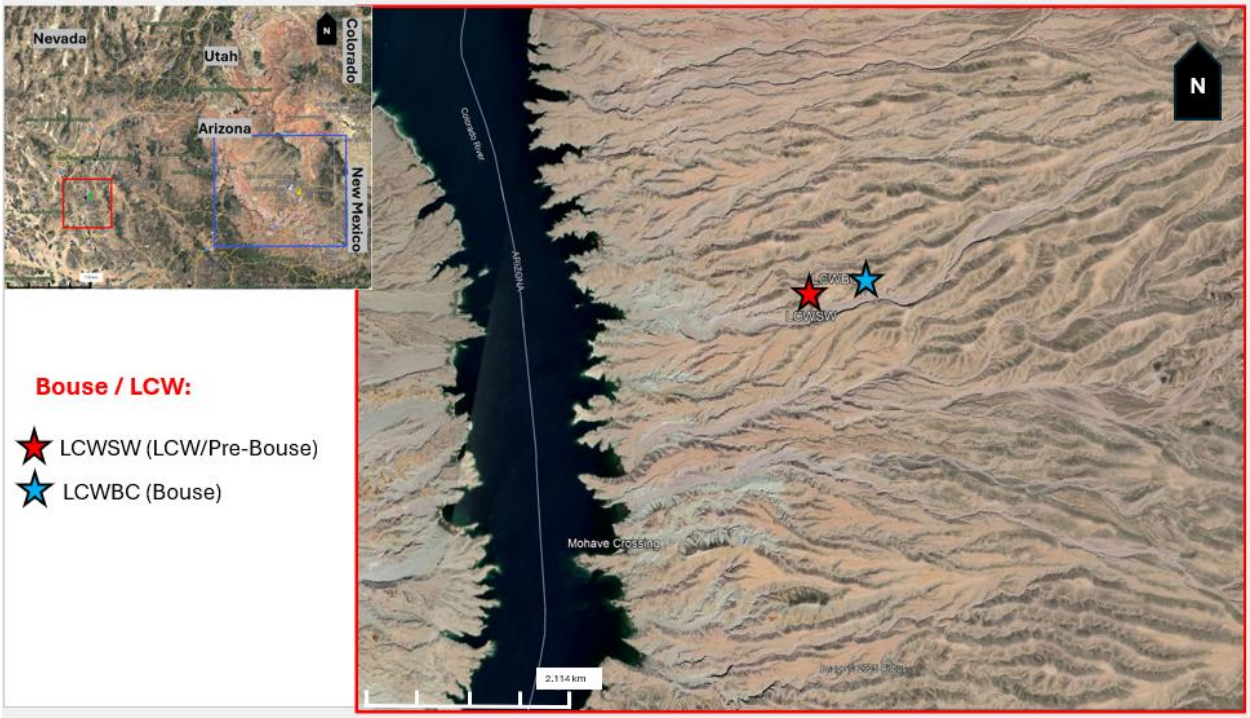


Figure 2: Location map showing where LCWSW and LCWBC samples are located within Cottonwood and Mohave Valleys.

The Blythe basin is the southernmost basin within this study. U-Pb dating at Hart Mine Wash dates a 4.8 Ma ash layer within the Bouse marl (Crow et al., 2025). Sanger

(2023) investigated the magnetostratigraphy of the Bouse Formation within Hart Mine Wash and found that there is a normal polarity section below the 4.8 Ma ash and a reverse polarity section immediately surrounding the ash, which continues for several meters up section in Bouse marl. This section was interpreted to represent the reversal period between the Sidufjall and Nunivak subchrons of the Gilbert Chron (Sanger., 2023). Additional samples were taken above and below the 4.8 Ma ash to perform a more robust reversal test.

GEOLOGIC BACKGROUND

The Colorado River is the main river system altering the landscape of the Colorado Plateau, with its headwaters in the Never Summer Mountains northwest of Lake Granby, Colorado. The river has incised and exhumed the flat lying strata of the Colorado Plateau at variable rates driven by tectonics and non-tectonic controls such as changes in climate, river capture, base level changes, and volcanism (Tanksi et al., 2025). The earliest known Colorado River deposits under Grand Mesa near modern day Grand Junction are 11 Ma (Aslan et al., 2019). Multiple constraints suggest that the Colorado River did not exit Grand Canyon until after between 6 and 4.8 Ma (Luchitta, 1972; Spencer et al., 2001; Faulds et al. 2016, Crow et. al. 2025) and first arrived to the Gulf of California between 4.8 and 4.6 Ma (Crow et al., 2021).

The Colorado Plateau experienced the majority of its uplift during the Laramide Orogeny, which began during the Late Cretaceous and was driven by the shallow subduction of the Farallon slab (Coney et al., 1976; Spencer et al., 1996, Roberts et al., 2012). Later stages of uplift occurred in the Oligocene, and some suggest that active uplift continues today, though the mechanisms that drive the ongoing uplift of the Colorado Plateau are still debated (Flowers et al., 2010; Karlstrom et al., 2022; Tanski et al., 2025). The increased Oligocene buoyancy may have resulted from enhanced asthenospheric upwelling following the detachment of the Farallon plate, where thermal expansion reduced the density of the crust and mantle lithosphere, leading to uplift of the Colorado

Plateau (Roy et al., 2009). Possible driver of ongoing uplift is edge-driven convection and mantle -flow in the Neogene and continuing into the present (Karlstrom et al., 2008; Moucha et al., 2008; van Wijk et al., 2010; Crow et al., 2011; Levander et al., 2011).

Since the Colorado Plateau has experienced continuing uplift since the Laramide, the presence of a basin on the Colorado Plateau is puzzling. The Bidahochi basin located on the Colorado Plateau would have needed to subside to create accommodation space for the paleo Hopi lake. He and Kapp (2023) suggest lithospheric drip beneath the Colorado Plateau as the main mechanism responsible for the subsidence that created the accommodation space needed for the Bidahochi basin.

Today the Colorado River follows a westward course through the Grand Canyon before reaching Lake Mead and the Basin and Range province, where it shifts to a southward trajectory into the Colorado River extensional corridor. The Colorado River extensional corridor, located between the California, Nevada, Arizona, and Mexico borders trends south-southeast in its upper half before shifting to a southwest direction near Chemehuevi and Parker Valley. This corridor has undergone multiple stress regimes and features various types of faults. Faults in this region include north–south–striking normal faults, as well as northwest–southeast–striking oblique-dextral to dextral-normal faults (Thacker et al., 2020). Low angle detachment faults are linked to the southern Basin and Range, which played a key role in accommodating early to middle Miocene crustal extension, leading to the formation of the corridor (Buising et al., 1990; Howard et al., 2007; Bennett et al., 2016; Dorsey et al., 2017). The early-middle Miocene period saw the most extension where the region was experiencing northeast directed extension with normal faulting present throughout. The late Miocene transitioned into northwest directed dextral shear where strike-slip faulting is also observed throughout the region (Mavor et al., 2023). Other contributing factors to the extension include the influence of the Farallon-North American arc system. Changes from compressional to extensional stresses occurred with the flattening of the subduction angle and associated asthenospheric upwelling, from the Farallon Plate (Cross and Pilger, 1978; Dickinson and Snyder, 1979; Buising, 1990; Howard et al., 2017).

Bidahochi Formation

The Bidahochi Formation is Miocene in age and is located on the Colorado Plateau in northeastern Arizona and northwestern New Mexico. Repenning and Irwin (1954) informally divided the Bidahochi into three separate members. The lower Bidahochi consists of banded gray, brown, and pink planar-bedded mudstone, as well as argillaceous fine-grained sandstone with intermittent rhyolitic ash beds. The lower member is interpreted to have been deposited in a playa/lacustrine environment. The middle member is volcanic and composed of mafic lava and tuff interfingered with mudstone, claystone, and sandstone toward the basin center and it likely erupted during or shortly after the deposition of the lower member. The upper member consists of white to pale brown, cross-bedded, poorly cemented, medium to fine-grained argillaceous sandstone, siltstones and claystones with tufa and beachrock at the upper parts. The upper members environment of deposition is more controversial and has been interpreted to be a fluvial dominated playa with some eolian deposits as well as more of a deep lacustrine system (Repenning & Irwin, 1954; Shoemaker et al., 1957; Douglass et al., 2020). These altering interpretations of the upper member all revolve around whether the ancestral Colorado river fed into the paleo Hopi lake, the paleo lake associated with the Bidahochi Formation. Shoemaker et al. (1957) further subdivided the Bidahochi into six units. The lower and middle members consist of units one through five while unit six comprises the entire upper formation of the Bidahochi.

Previous Geochronological Studies (Bidahochi)

There are multiple fallout ash beds preserved throughout the Bidahochi Formation, which can be used as basin-wide correlation horizons and for geochronological analysis. The oldest identified ash beds were deposited ~14 meters above the base of the formation (Dallegge et al., 2003). Of these identified ash beds, the oldest ash bed recorded in the lower member of the Bidahochi was dated using biotite $^{40}Ar/^{39}Ar$ geochrology at 15.46 ±

0.36 Ma, modeled glass $^{40}Ar/^{39}Ar$ dating at 15.8 Ma, was geochemically correlated to the 15.84 ± 0.05 Ma Echo Spring Mountain felsic ash bed (Dallegge et al., 2003). Two young ash beds have been dated within the upper member of the Bidahochi. One identified at Greasewood was geochemically correlated to the 6.62 ± 0.05 Ma Blacktail Creek ash (Dallegge et al., 2003). The second airfall tuff that was dated at 6.69 ± 0.16 Ma by K-Ar dating and was found at White Cone and correlated to Roberts Mesa (Scarburough et al., 1974). However, there are two ash beds stratigraphically higher than the 6.62 Ma ash bed that have recently yielded preliminary data that are used within this project (Crow, personal communication). There is also a recently dated detrital sanidine $^{40}Ar/^{39}Ar$ MDA age of 6.07 ± 0.07 that was found in the upper Bidahochi near Roberts Mesa (Heizler et al., 2021). The only previous paleomagnetic study suggested that sedimentation ceased within the closed basin of the Bidahochi around 5.59 Ma, based on fossil data and the highest paleomagnetic reversal located within White Cone Peak, which preserves portions of the upper Bidahochi Formation (Lindsay et al., 1984). Paleomagnetic data reported here is from nearby sites and includes stratigraphically higher strata.

Within White Cone, twenty-two sites were collected by Lindsay et al. (1984) within the 70-meter outcrop consisting of the upper Bidahochi, and magnetostratigraphy revealed two relatively long normal polarity chrons in the upper part of White Cone and one poorly defined short normal polarity chron, which suggests the Bidahochi at White Cone was deposited between 7.26 and 6.02Ma, as shown in **Figure 3.** An airfall tuff in the middle member yielded a K-Ar date of 6.69 ± 0.16 Ma, which was used to constrain the section relative to the GPTS (Scarburough et al., 1974). However, the error in the 6.69 ± 0.16 Ma suggests it could be as young as 6.53 Ma or as old as 6.85 Ma which could place the airfall tuff within the R2 or the N2 defined chrons by Lindsay et al. (1984). The tuff was not sampled for paleomagnetic analysis therefore the polarity is not known. This airfall tuff was also correlated to Roberts Mesa and used as a bracket point within the Roberts Mesa section in this study.

Lindsay et al. (1984) reported that paleomagnetic samples from the White Cone locality exhibited a strong magnetic overprint that was difficult to remove using the

demagnetization techniques available at the time. However, modern demagnetization methods offer significantly higher sensitivity and resolution than those used four decades ago. As a result, the magnetostratigraphic interpretations presented in this study are considered more reliable and confidently constrained.

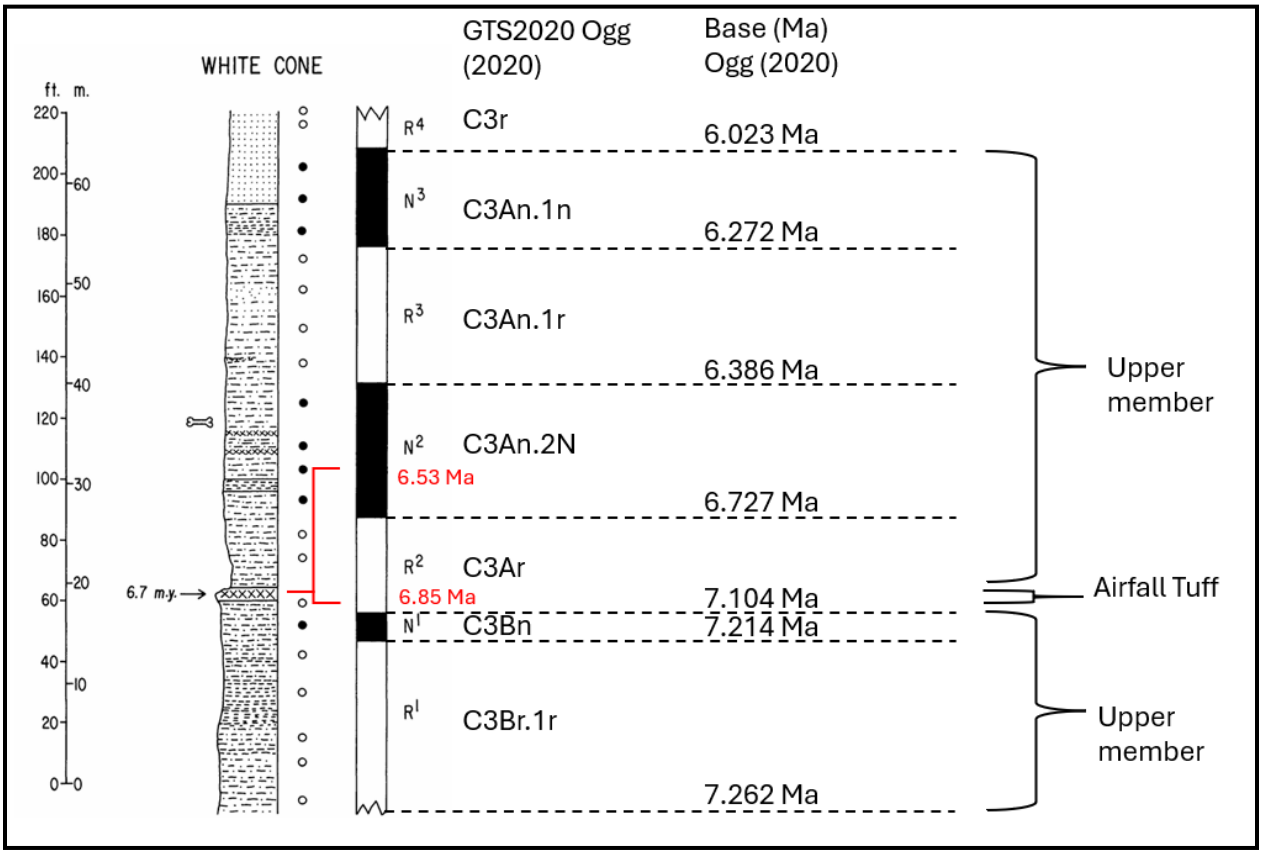


Figure 3: Modified from (Lindsay et al., 1984). Figure of White Cone with the GPTS superimposed.

Bouse Formation

The Pliocene Bouse Formation is found in southeastern California, western Arizona, and southern Nevada, and consists of bedded marl, bioclastic limestone, tufa, siltstone, claystone, and fine silty sandstone. These lithologies are representative of the arrival of the Colorado River within the lower Colorado River (LOCO) valley and record the evolution of closed basins that were eventually filled by the early Colorado River, leading to the formation of a series of lakes separated by natural dams (House et al., 2008). The Bouse is

unconformably overlain by the Bullhead alluvium and onlaps onto alluvial fans and bedrock hillslopes. The Bouse Formation can be observed in outcrops up to 50 meters thick and in subsurface wells up to 250 meters thick (Howard et al., 2016; Cohen et al., 2019).

Previous Geochronological Studies (Bouse)

Prior geochronological work has been conducted along the LOCO establishing dates that have constrained the arrival of the Colorado River as seen in **Figure 4** (Crow et al., 2021). Starting in the northernmost Lake Mead area of the LOCO, the arrival of the Colorado River is bracketed between 6.0 Ma and 4.7 Ma (Crow et al., 2021). The 6.0 Ma comes from an ash date within the non-Colorado-River-derived Hualapai Limestone which yielded a $^{40}Ar/^{39}Ar$ biotite age of 5.97 ± 0.07 Ma at 2σ uncertainty (Spencer at al., 2021). Glass shard analysis was also done on younger ashes interbedded in pre-Colorado River deposits in an isolated basin in the Lake Mead area and correlated to the Conant Creek Tuff which yielded a $^{40}Ar/^{39}Ar$ age of 5.62 ± 0.11Ma (Faulds et al., 2016). New preliminary results also suggest that a pre-Bouse ash near Hoover Dam could be as young as 4.8 Ma (Crow et al., 2025). Constraints from ancestral Colorado River deposits suggest that integration happened before 4.7 Ma as a basaltic flow interbedded in Grand Wash gravels graded to the Colorado River which yielded a date of 4.73 ± 0.17 Ma (Crow et al., 2019). The Sandy Point basalt $^{40}Ar/^{39}Ar$ age of 4.49 ± 0.46 which overlies post-integration Colorado River gravel of the Bullhead Alluvium is found within the Grand Wash Trough (Faulds et al., 2016). In summary these constraints suggest that that Colorado River integration to the Lake Mead area occurred between 4.8 and 4.7 Ma.

The Colorado River arrival into Cottonwood Valley and Mohave Valley is bracketed between 5.7 Ma and 4.1 Ma (Crow et al., 2021). The later date comes from multiple ashes identified within pre-Bouse deposits in the Lost Cabin beds that have been correlated to the 5.7 Ma Wolverine Creek eruption which predates the arrival of the Colorado River and another ash date, 4.1 Ma, which postdates the arrival of the river (House et al., 2008; Crow

et al., 2021). Schwing's (2019) magnetostratigraphic study supports the established geochronological framework by identifying a magnetic reversal and correlating the majority of the pre-Bouse Lost Cabin beds to the reversed Gilbert (C3r) subchron, which spans from 6.023 to 5.235 Ma. The identified reversal is interpreted as the transition from the reversed C3r subchron to the normal Thvera (C3n.4n) subchron. This interpretation is further constrained by three $^{40}Ar/^{39}Ar$-dated tephra layers in the Lost Cabin beds—5.59 ± 0.05 Ma, 5.49 ± 0.79 Ma, and 5.35 ± 0.07 Ma—all of which fall within the reversed Gilbert (C3r) subchron (Crow et al., 2021). These data collectively indicate that the arrival of the Colorado River in these valleys occurred during or after the Thvera (C3n.4n) subchron (House et al., 2008; Schwing, 2019; Crow et al., 2021).

Magnetostratigraphic work done by Sanger (2023) in Mohave Valley places Bouse deposits within the Park Moabi section in the Thvera (C3n.4n) subchron. Sanger (2023) came to this conclusion based on Schwing's (2019) finding that pre-Bouse Lost Cabin beds were deposited at the beginning of the Thvera subchron and the normal polarity results at Park Moabi. This hypothesis however is challenging to confirm because there are no geochronological dates within the Park Moabi section. In the absence of a reversal test within this location, the normal polarity interval recorded within the Mohave section could lie within the Thvera (C3n.4n) subchron or alternatively within the younger Sidufjall (C3n.3n) subchron.

Within the Blythe basin, detrital sanidine dating has been used to constrain the maximum depositional age of the Bouse Formation. Three samples taken throughout the Bouse Formation yielded dates that were younger than 5.3 Ma. Two DS grains out of the total 534 DS grains yielded a MDA of 4.7 Ma for the lower Bouse Formation (Crow et al., 2021). In a similar study, probable ash beds at three locations in lower Bouse Formation (including Hart Mine Wash) yielded a significant population of young zircon grains with an age of 4.8 Ma (Crow et al., 2025). The normal polarity Lawlor tuff within the Blythe basin is found interbedded within the basal carbonate member of the Bouse at high elevation in the Blythe basin and yields a $^{40}Ar/^{39}Ar$ date of 5.0 to 4.9 Ma (Sarna-Wojcicki et al., 2011). Magnetostratigraphic work done by Sanger (2023) on lower Bouse Formation in Hart Mine

Wash, where the probable ash was recently dated at 4.8 Ma places the Bouse there within the Sidufjall (C3n.3n) subchron as well as the transition into the C3n.2r reverse subchron. These magnetostratigraphy results combined with the DS further support that the Colorado River arrived in the Blythe basin during and after the Sidufjall (C3n.3n) subchron. Sanger (2023) also completed a magnetostratigraphic study within the northern part of the Blythe basin at Mesquite Mountain which yielded all normal polarity samples and is interpreted to lie within the normal Sidufjall (C3n.2n) subchron. Howard et al., (2016) compiled previous magnetostratigraphic work done by Malmon et al. (2011a) near Mesquite Mountain in the northern Blythe basin where a normal to reverse polarity interval was found near a disconformity. Further work is needed to correlate this result with those conducted by Sanger (2023) at a nearby site.

Within the Fish-Creek Vallecito basin, a northern basin of the evolving proto Gulf of California, the arrival time of the Colorado River is debated (Crow et al., 2021; Dorsey et al., 2018; Dorsey et al., 2011). The marine Wind Caves member of the Latrania formation of the Imperial group records the arrival of the Colorado River within the Fish-Creek Vallecito basin (Hanna, 1926; Winker and Kidwell, 1996). Recent study by Crow et al. (2021) suggests that the Colorado River reached the Gulf of California between 4.80 – 4.63 Ma which is correlated to the reverse subchron C3n.2r. Previous magnetostratigraphic data within this same basin reports the Wind Caves member to be within the reverse C3r Gilbert chron (Dorsey et al., 2007, 2011). This magnetostratigraphic data is hung on ~2 Ma year old ash dates located high within a 5 km thick section (Dorsey et al., 2011). This magnetostratigraphic work is challenging to confirm due to the thickness of the section and the for potential repeated section due to normal faulting within the area. All relevant magnetostratigraphic work within the LOCO was summarized within **Figure 18** to help better visualize and understand the timing of arrival into these valleys.

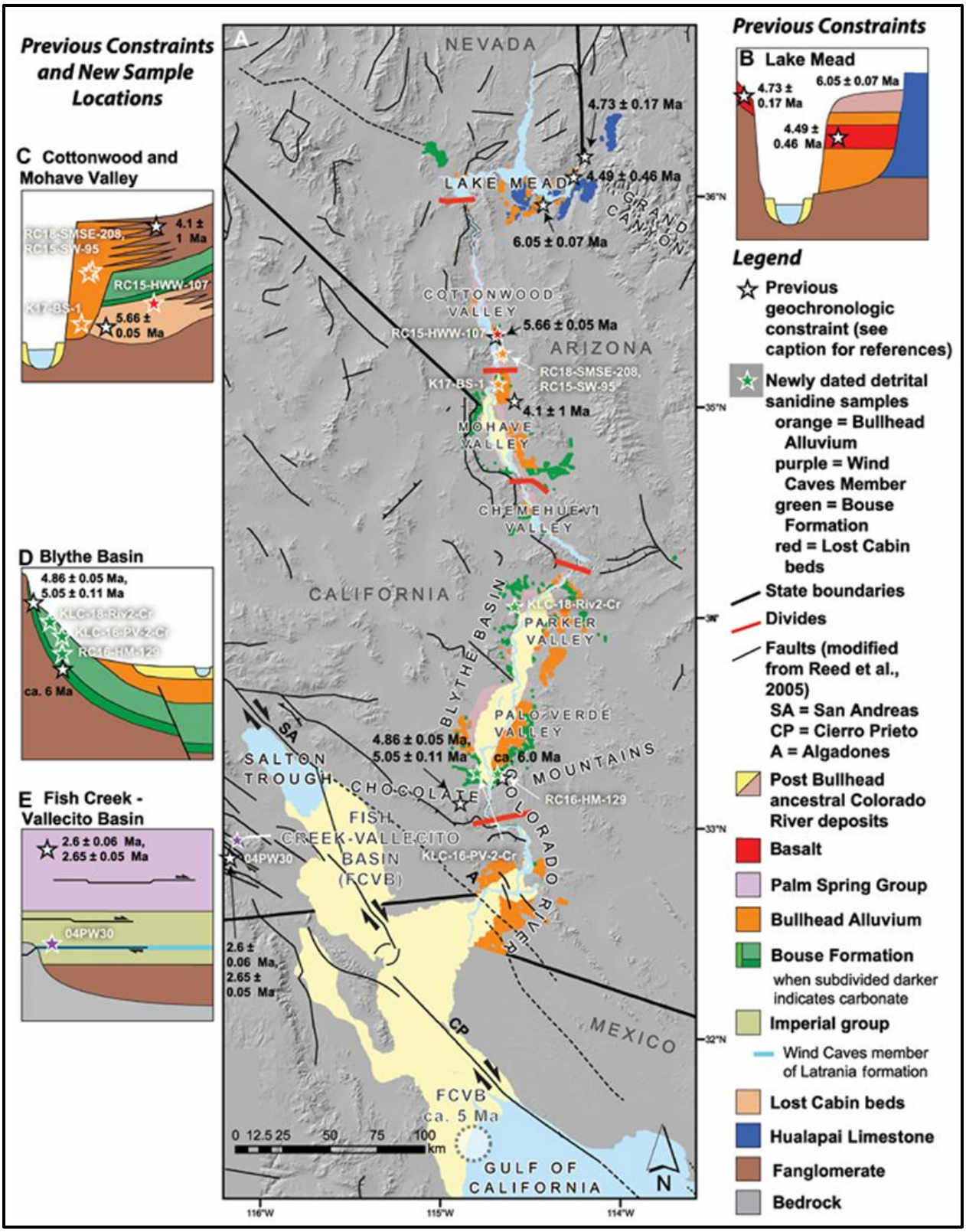


Figure 4: Figure from Crow et al., (2021) A: summarizes the previously completed geochronological studies on the LOCO showing sampling locations and outcrops of pre- and post-Colorado River deposits. B-E: show depositional relationships, previous sampling locations, and structures within the LOCO.

METHODS

Field Sampling

Magnetostratigraphic field sampling was conducted in May of 2024, at two key outcrops of the upper Bidahochi Formation, Roberts Mesa and Greasewood, in northeast Arizona **(Figure 1).** Most of the rocks within Roberts Mesa and Greasewood were too friable to drill with a portable gas-powered chainsaw modified with a Pomeroy coring device. Instead, we used a Brunton compass to orient the block samples. All the blocks collected had a minimal dip between 0 and 3 degrees. Some coarser-grained samples were taken in larger blocks, oriented in the field, and later drilled in the lab using a Griffin coring device.

Sampling was conducted at fourteen sites within the Roberts Mesa section (RM1–RM14), with up to three samples collected per site depending on the degree of lithification. At some locations, poorly lithified and friable sediments limited recovery, resulting in only one or two usable samples. In cases where the material was too friable to be drilled or cut in the lab, the site was not able to be used for analysis. Sampling within the Roberts Mesa section focused on the upper member of the Bidahochi and the average vertical distance between the sites ranged from 1-2 m to 10-20 m, dictated by viable outcrop availability.

Additional samples were taken approximately fourteen miles from Roberts Mesa where sampling was conducted at fourteen sites within the Greasewood outcrop (GW0 through GW13), yielding three samples per site depending on the degree of lithification of each site. Sampling within the Greasewood outcrop focused on the upper member of the Bidahochi Formation and the average vertical distance between the sites ranged from 1-2 m to 10-30 m, also dictated by viable outcrop availability.

Bouse Formation sediments were collected in the field within Hart Mine Wash in 2023 by Ryan Crow in the Blythe basin (LOCO) **Figure 5.** These samples were taken in block samples and oriented in the field. Pre-Bouse Lost Cabin Beds (LCWSW) were collected in Lost Cabin Wash within Cottonwood Valley, west of Lake Mohave in the LOCO. Bouse

formation sediments were also taken within a fluvial incision site that was interpreted to be a fluvially incised channel in the Lost Cabin Beds that hold Bouse deposits (LCWBC). Both locations (LCWSW & LCWBC) were taken by Schwing, Crow, and Dulin in 2019 and were taken in block samples and oriented in the field. A map is seen in **Figure 2** showing the location of the two Lost Cabin Bed sites.

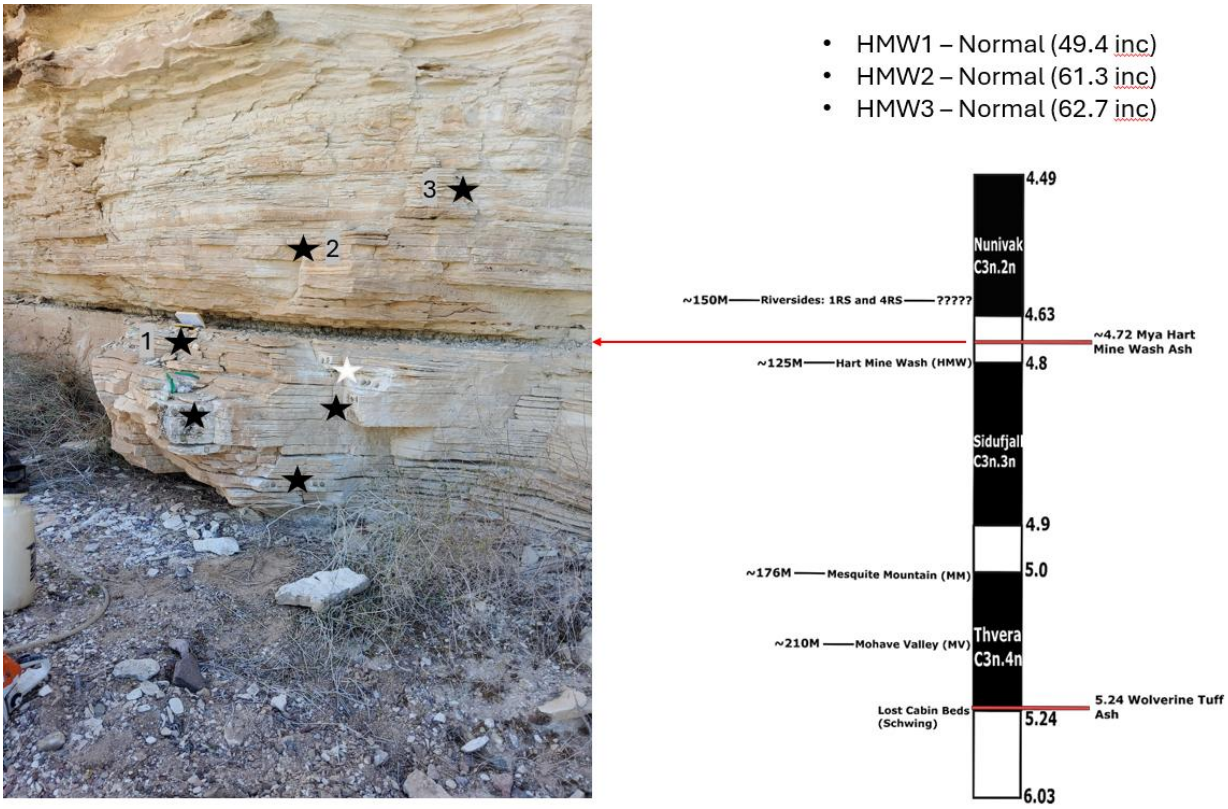


Figure 5: Location of HMW1 – HMW3 in relation to the HMW ash. GPTS is modified from Sanger (2023). Black stars indicate a site with normal polarity inclinations and white stars indicate reverse polarity inclinations.

Sample Preparation

Since the majority of the samples collected were poorly lithified, they were taken in blocks and oriented in the field. Extra care was taken when cutting these samples using a band saw with a demagnetized saw blade to avoid inducing or altering the samples' magnetic fabric. The samples were cut into 2 cm cubes, sanded by hand, and placed in a

clear, plastic, 8 cm^3 demagnetized box for magnetic analysis (following Butler, 1992). If a specimen was difficult to cut, smaller pieces were taken and placed in the clear, plastic 8 cm^3 box with a piece of shop rag to hold the sample in place and inhibit sample reorientation.

Samples that were indurated and lithified enough were able to be drilled with a water-cooled Pomeroy coring device using a steel diamond coring attachment. The cored samples were then cut to 2.2 cm for further analysis. These cores were cut using a small wet saw that utilizes steel blades to avoid alteration of the magnetic fabric within the core. All samples were then marked with a north arrow on the top of plastic demagnetized block as well as the side to properly orient them for analysis. All of the samples' magnetic directions from the Lost Cabin Wash and some from the Hart Mine Wash were analyzed using a 2G enterprises cryogenic magnetometer with DC squids at the University of Oklahoma, which is housed inside a magnetically shielded room to avoid magnetic interference and prevent the sample from acquiring the Earth's modern magnetic field direction. The cryogenic magnetometer utilizes an automated sample handler, which houses and measures the specimen in three directions, x, y, and z.

Demagnetization was performed using AF (Alternating Field) demagnetization which is a destructive process by measuring the decay of magnetic grains within the sample. All AF demagnetization was performed at New Mexico Highlands University in Las Vegas, NM. The orthogonal coil AF demagnetizer is in line with an Applied Physics 755-4K cryogenic magnetometer, which automatically measures the remaining specimen magnetization after each step of the AF treatment. Demagnetization was conducted in 25 steps using a modified sequence that is best used when analyzing sedimentary rocks (0mT-20mT, 2mT increments and 20mT-100mT, 5mT increments). Sedimentary rocks tend to decay more rapidly due to the relatively weak nature of the Natural Remanent Magnetization (NRM) in these samples, so the modified sequence was used to help capture these small incremental changes.

Super IAPD software was used in determining magnetic components. The graphic results of AF demagnetization are magnetic decay curves, where it decays towards the origin, resulting in an inclination and declination. The magnetization components were determined using orthogonal vector projections (Zijderveld., 1967) and group statistics are visualized via an equal area plot (Butler., 1992; Love, Jeffrey., 2007; Fisher., 1953). Super IAPD was also used for Principal Component Analysis (PCA) and Fisher statistics to determine site means.

Rock Magnetic Study

Curie Temperature Analysis

Rock magnetization tests are conducted by acquiring Curie temperatures through thermomagnetic curve analysis. The machine used to heat and cool samples through their Cure temperature is an AGICO KLY5 kappa bridge paired with a CS-4 furnace attachment (Agico, Inc.). The CS-4 furnace attachment monitors the magnetic response of the specimen's magnetic carriers as temperature increases from room temperature to 700°C. To prevent oxidation, which can alter magnetic mineralogy, the measurements are performed in an argon gas atmosphere. Specimens are powdered and approximately weighed to 0.500 grams before being placed in a quartz tube, where a thermometer is inserted to track temperature changes in the sample. This process generates a temperature curve that indicates the Curie temperature of the magnetic minerals in the specimen (**Figures 11-14).** The temperature curves are then analyzed and corrected using Cureval8 (Agico, Inc.), which removes the effect of the quartz tube on the magnetic remanence measurement by applying a known standard value for the quartz tube's remanence.

RESULTS

Quality Analysis (Grading)

The quality of data output by orthogonal vector projections (Zijderveld., 1967) were graded using a letter grade scale, A through F (using the same qualitative criteria used in

Schwing (2019) and Sanger (2023)). First, each sample was graded and then the site was graded using an average of the three samples (three samples per site). An A letter grade represents a sample that shows a stable trend in the decay curve, decays toward the origin, and has a clear linear direction of a Characteristic remanent magnetization (ChRM), with little to no point clustering (**Figure 6).** A B letter grade represents a sample that has an increase in point clustering but still shows an overall linear decay curve, decays towards the origin, and has a clearly defined ChRM. **(Figure 7).** A C letter grade represents a sample that displays clustering of data toward the origin but not entirely reaching the origin. **(Figure 8).** A D letter grade represents a sample which does not decay towards the origin and does not have a clear direction of a ChRM. **(Figure 9).** An F letter grade represents a sample that does not decay towards the origin, has no clear direction, and the point clustering is scattered. **(Figure 10).** F quality data lacks any reasonable interpretation; thus, the data is too poor to even be considered in statistical analysis.

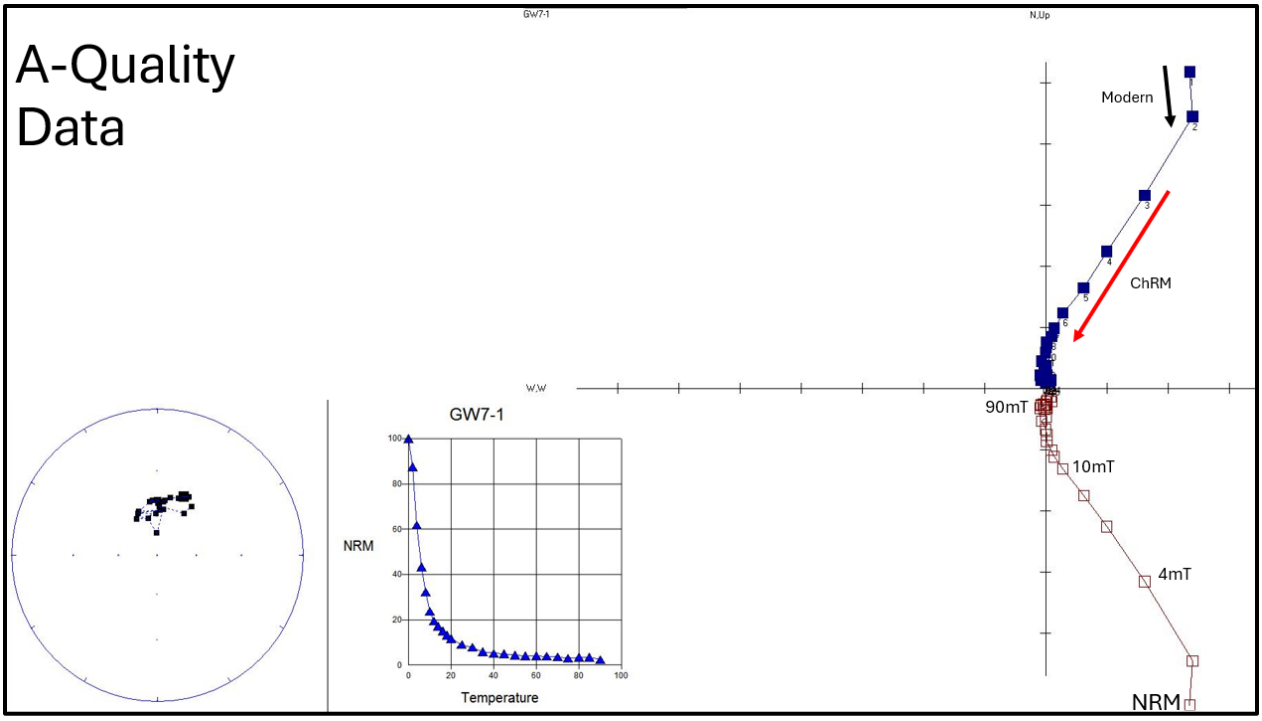


Figure 6: Representative Zijderveld [1967] diagrams and equal area projections used for this study. Closed boxes represent declination values and open boxes represent inclination values. NRM and ChRM are both labeled. A quality data shown.

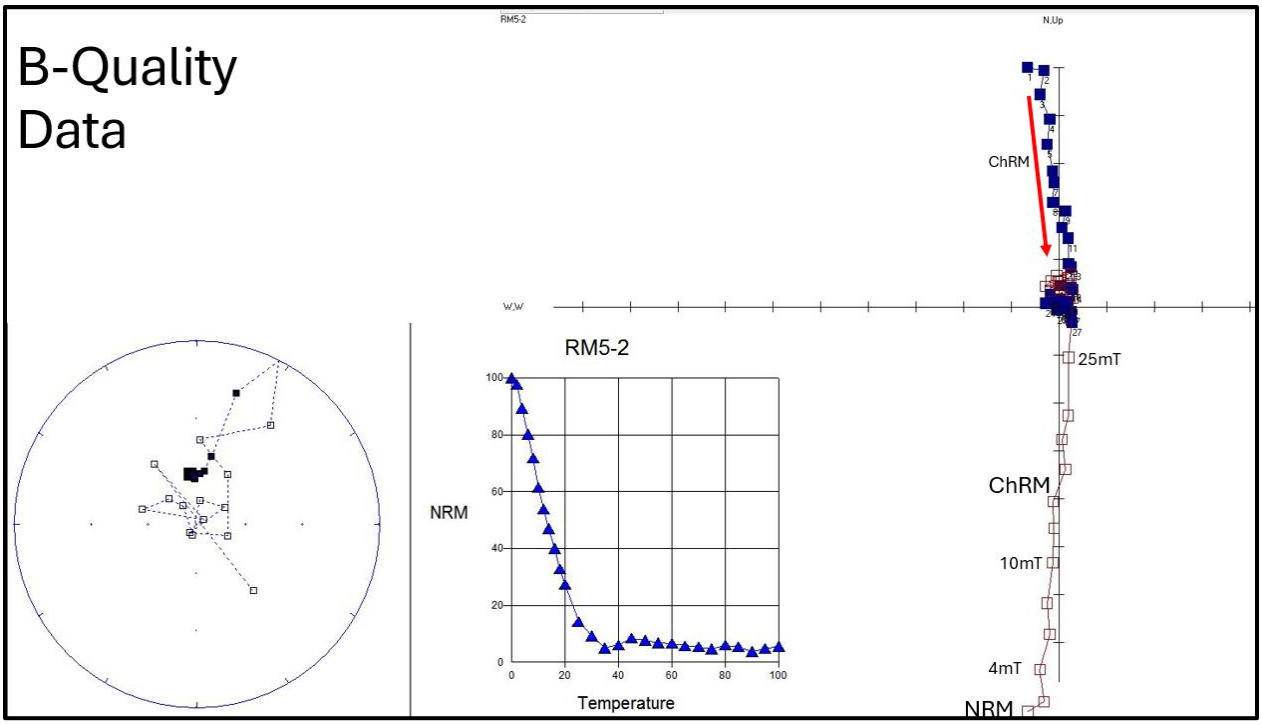


Figure 7: Representative Zijderveld [1967] diagrams and equal area projections used for this study. Closed boxes represent declination values and open boxes represent inclination values. NRM and ChRM are both labeled. B quality data shown.

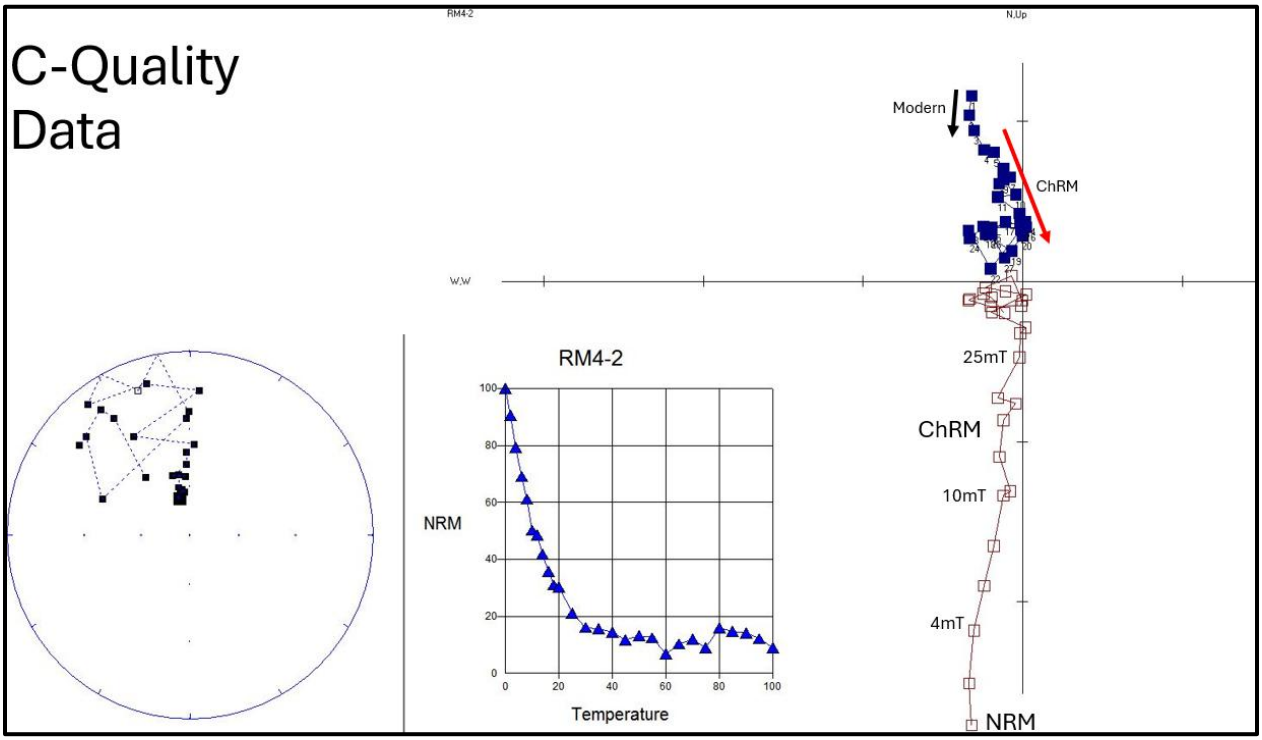


Figure 8: Representative Zijderveld [1967] diagrams and equal area projections used for this study. Closed boxes represent declination values and open boxes represent inclination values. NRM and ChRM are both labeled. C quality data shown.

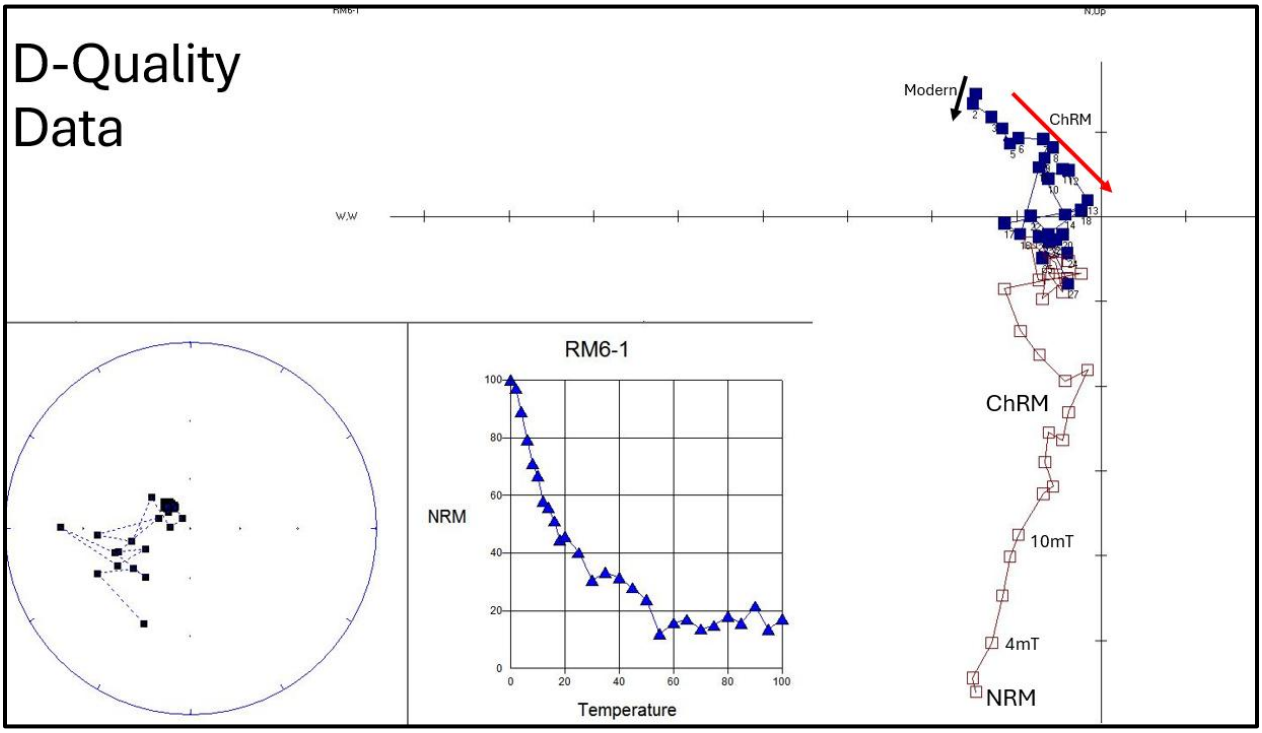


Figure 9: Representative Zijderveld [1967] diagrams and equal area projections used for this study. Closed boxes represent declination values and open boxes represent inclination values. NRM and ChRM are both labeled. D quality data shown.

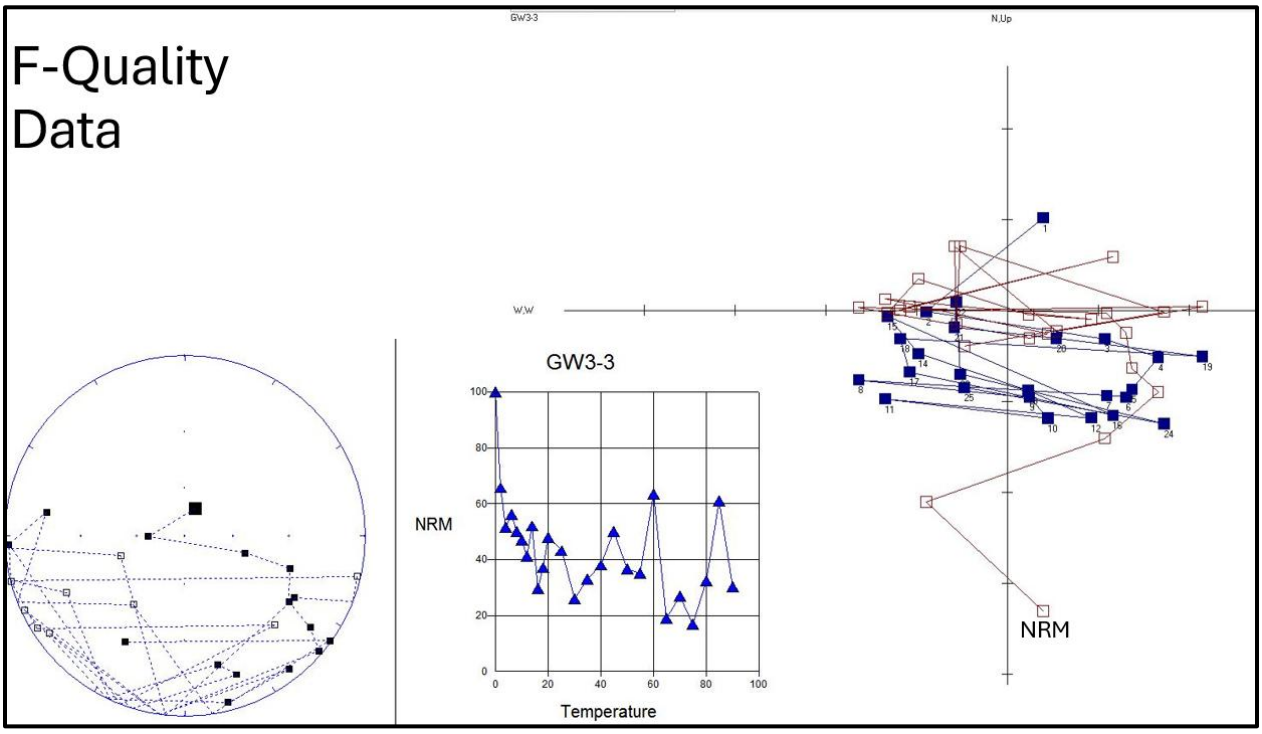


Figure 10: Representative Zijderveld [1967] diagrams and equal area projections used for this study. Closed boxes represent declination values and open boxes represent inclination values. F quality data shown.

Magnetostratigraphy

Roberts Mesa

Alternating field demagnetization within the Roberts Mesa location yielded 30/39 (N/No) samples that had stable demagnetizations with a presence of a characteristic remanent magnetization (ChRM) **(Table 1)**. The number of samples used within the site shown as N/No where N is the number of samples used in analysis and No is the total amount of samples collected. The N/No was determined using the quality analysis grading where samples that were given F quality were not used in statistical analysis. Alternating field samples yielded a declination, inclination, and a maximum angular deviation angle (MAD), while site mean statistics yielded a declination, inclination, MAD angle, α95, and a K-value.

Principal component analysis was performed on each sample from Roberts Mesa to extrapolate whether the sample revealed a positive or negative inclination, thus revealing whether the sample was deposited in a normal or reverse polarity subchron. Sites were numbered starting at the base of the section (RM1 = 1900 MASL; RM14 = 1959 MASL) and were sampled where consolidated beds were available. Sites RM1 through RM3 yielded all positive inclinations ranging from 76.4° to 49.2°. Site RM1's group statistics yielded an average inclination of 67.1°, a MAD angle of 14.6°, and a K-value of 72.27. Site RM2's group statistics yielded an average inclination of 76°, a MAD angle of 27.2°, and a K-value of 21.67. Site RM3 had one sample that was not used in the group statistics because of poor data quality (RM3-2), therefore only two samples were used for group statistics. This site's group statistics yielded an average inclination of 55.6°, a MAD angle of 51.3°, and a K-value of 25.81.

Site RM4 yielded two samples with positive inclinations (RM4-1: 70.3° & RM4-2: 71.7°) and one sample with a negative inclination (RM4-3: -37.9°). Site RM5 also yielded two samples with positive inclinations (RM5-2: 62.4° & RM5-3: 54.5°) and one sample with

a negative inclination (RM5-1: -44.2°). Group statistics were not run on these two sites because of the presence of both positive and negative inclination values.

Sites RM6 through RM14 yielded all positive inclinations ranging from 78.5° to 14.8°. Site RM6's group statistics yielded an average inclination of 60.3°, a MAD angle of 96.5°, and a K-value of 2.75. Site RM7's group statistics yielded an average inclination of 60.3°, a MAD angle of 12.5°, and a K-value of 98.16. Site RM8 only yielded one out of three samples that were used in analysis (RM8-1) with an inclination of 78.5°. Site RM10's group statistics yielded an average inclination of 69.4°, a MAD angle of 57.5°, and a K-value of 5.67. Site RM11's group statistics yielded an average inclination of 58.9°, a MAD angle of 10.2°, and a K-value of 147.69. Site RM13's group statistics yielded an average inclination of 81.6°, a MAD angle of 75.3°, and a K-value of 3.77. Sites RM9, RM12, and RM14 were all assigned as F quality data therefore, they were not included in analysis.

Greasewood

Alternating field demagnetization within the Greasewood location yielded 24/42 (N/No) samples that had stable demagnetizations with a presence of characteristic remanent magnetization **(Table 2)**. The same quality analysis and statistical analysis that was run on Roberts Mesa was also run on the Greasewood location. The same site numbering convention begins at the base of the exposed section GW0 (1866 masl) through GW13 (1946 masl).

GW0 revealed positive inclinations throughout, and the group statistics yielded an average inclination of 72.5°, a MAD angle of 24.6°, and a K-value of 26.15.

Site GW2's samples yielded all three of its samples within the site to have negative inclinations. This site's group statistics yielded an average inclination of -10.6°, a MAD angle of 53.7°, and a K-value of 6.34. Site GW4 yielded two samples with negative inclinations (GW4-1: -5.7° & GW4-2: -4.6°) and one sample with a positive inclination (RM4-3: 55.6°).

Sites GW5 through GW9 yielded all positive inclinations ranging from 67.4° to 31.6°. Sites GW5's group statistics yielded an average inclination of 63.6°, a MAD angle of 10.1°, and a K-value of 151.32. Sites GW6's group statistics yielded an average inclination of 67.5°, a MAD angle of 91.4°, and a K-value of 2.92. Sites GW7's group statistics yielded an average inclination of 45.1°, a MAD angle of 16.5°, and a K-value of 56.7. Sites GW8's group statistics yielded an average inclination of 63°, a MAD angle of 12°, and a K-value of 106.25. Sites GW9's group statistics yielded an average inclination of 64.5°, a MAD angle of 77.4°, and a K-value of 3.62. Sites GW1, GW3, and GW10-13 were all assigned as F quality data therefore, they were not able to be analyzed due to poor data quality.

Hart Mine Wash (HMW)

Alternating field demagnetization was performed on Bouse deposits within Hart Mine Wash (HMW) in the Blythe Basin located in the LOCO **(Table 3)**. The HMW samples yielded 9/9 (N/No) samples that had stable demagnetizations. All three sites within Hart Mine Wash (HMW1-HMW3) yielded positive inclinations. Site HMW1 yielded an average inclination of 49.4°, a MAD angle of 7.7°, and a K-value of 260.28. Site HMW2 yielded an average inclination of 61.3°, a MAD angle of 27.3°, and a K-value of 21.4. Site HMW3 yielded an average inclination of 62.7°, a MAD angle of 31.2°, and a K-value of 16.64.

Lost Cabin Wash (LCWBC & LCWSW)

Alternating field demagnetization was performed on pre-Bouse deposits (LCWSW) and Bouse deposits found in a fluvial incision site (LCWBC) **(Table 4-5)**. LCWBC yielded 9/9 (N/No) samples that had stable demanganizations and yielded two sites with negative inclinations (LCWBC2 & LCWBC4) and one site with positive inclinations (LCWBC3).

Site LCWBC2 group statistics yielded an average inclination of -21.8°, a MAD angle of 11.6°, and a K-value of 114.88. Site LCWBC4 group statistics yielded an average inclination of -32.7°, a MAD angle of 9.7°, and a K-value of 163.99. Site LCWBC3 was the only site that yielded positive inclinations with an average inclination of 72.7°, a MAD angle of 65.2°, and a K-value of 4.65.

LCWSW yielded 7/9 (N/No) samples that had stable demanganizations and yielded three sites with negative inclinations. Site LCWSW1 had only one sample within the site that had a stable demagnetization (LCWSW1-2), so group statistics were not run. Site's LCWSW2 and LCWSW3 both yielded negative inclination values. Site LCWSW2 yielded an average inclination of -43.4°, a MAD angle of 9.7°, and a K-value of 162.05. Site LCWSW3 yielded an average inclination of -39.1°, a MAD angle of 9.7°, and a K-value of 162.38.

Sample Name	Demag	Polarity	Declination	Inclination	MAD	Rank	Alpha 95	K(Site)	N/No
RM1-1	AF	N	348.7	76.4	7.7	A			
RM1-2	AF	N	326.3	64.1	7.8	A			
RM1-3	AF	N	326.3	60	8.2	A			
Site	**AF**	**N**	**330.8**	**67.1**	**14.6**	**A**	**14.6**	**72.27**	**3/3**
RM2-1	AF	N	316.1	68.8	14.4	C			
RM2-2	AF	N	316.7	78.6	9.2	C			
RM2-3	AF	N	227.1	65.4	11.3	C			
Site	**AF**	**N**	**280**	**76**	**27.2**	**C**	**27.2**	**21.67**	**3/3**
RM3-1	AF	N	309.5	59.4	6.5	A			
RM3-2	AF	N/A	N/A	N/A	N/A	F			
RM3-3	AF	N	274.3	49.2	4.1	A			
Site	**AF**	**N**	**289.7**	**55.6**	**51.3**	**B**	**51.3**	**25.81**	**2/3**
RM4-1	AF	N	320.4	70.3	8.5	B			
RM4-2	AF	N	346.6	71.7	8.1	B			

RM4-3	AF	R	190.7	-37.9	9.5	B			
Site	**AF**	**N**	**N/A**	**N/A**	**N/A**	**B**	**N/A**	**N/A**	**3/3**
RM5-1	AF	R	151.4	-44.2	4.9	A			
RM5-2	AF	N	354.2	62.4	3.7	B			
RM5-3	AF	N	0.2	54.5	5.5	B			
Site	**AF**	**N**	**N/A**	**N/A**	**N/A**	**A**	**N/A**	**N/A**	**3/3**
RM6-1	AF	N	309.2	65.9	4.9	D			
RM6-2	AF	N	331.7	53.5	7.2	B			
RM6-3	AF	N	72	14.8	5.4	C			
Site	**AF**	**N**	**16.6**	**60.3**	**96.5**	**C**	**96.5**	**2.75**	**3/3**
RM7-1	AF	N	344.8	55.1	6.7	A			
RM7-2	AF	N	330.3	63.2	7.4	A			
RM7-3	AF	N	359.5	61	6.6	A			
Site	**AF**	**N**	**345.2**	**60.3**	**12.5**	**A**	**12.5**	**98.16**	**3/3**
RM8-1	AF	N	322.5	78.5	12.8	C			
RM8-2	AF	N/A	N/A	N/A	N/A	F			
RM8-3	AF	N/A	N/A	N/A	N/A	F			
Site	**AF**	**N**	**N/A**	**N/A**	**N/A**	**D**	**N/A**	**N/A**	**1/3**
RM9-1	AF	N/A	N/A	N/A	N/A	F			
RM9-2	AF	N/A	N/A	N/A	N/A	F			
RM9-3	AF	N/A	N/A	N/A	N/A	F			

Site	AF	N/A	N/A	N/A	N/A	F	N/A	N/A	0/3
RM10-1	AF	N	347.9	44.8	12.8	C			
RM10-2	AF	N	110.4	56	15.4	D			
RM10-3	AF	N	63	70.9	14.5	D			
Site	**AF**	**N**	**45.8**	**69.4**	**57.5**	**D**	**57.5**	**5.67**	**3/3**
RM11-1	AF	N	317.8	64.9	5.7	A			
RM11-2	AF	N	326.6	53	4.1	A			
RM11-3	AF	N	329.7	58.6	4.8	A			
Site	**AF**	**N**	**325.3**	**58.9**	**10.2**	**A**	**10.2**	**147.69**	**3/3**
RM12-1	AF	N/A	N/A	N/A	N/A	F			
Site	**AF**	**N/A**	**N/A**	**N/A**	**N/A**	**F**	**N/A**	**N/A**	**0/1**
RM13-1	AF	N	14.2	60.6	3.4	A			
RM13-2	AF	N	158.3	39.4	3.0	A			
RM13-3	AF	N	251.5	69.4	1.4	A			
Site	**AF**	**N**	**168.3**	**81.6**	**75.3**	**A**	**75.3**	**3.77**	**3/3**
RM14-1	AF	N/A	N/A	N/A	N/A	F			
RM14-2	AF	N/A	N/A	N/A	N/A	F			
Site	**AF**	**N/A**	**N/A**	**N/A**	**N/A**	**F**	**N/A**	**N/A**	**0/2**
Overall	**AF**								**30/39**

Table 1 ChRM's for Roberts Mesa (RM) location

Sample Name	Demag	Polarity	Declination	Inclination	MAD	Rank	Alpha 95	K(Site)	N/No
GW0-1	AF	N	350.3	59.4	8.7	A			
GW0-2	AF	N	12.6	72.1	4.7	B			
GW0-3	AF	N	75.2	77.4	5.7	B			
Site	**AF**	**N**	**12.6**	**72.5**	**24.6**	**B**	**24.6**	**26.15**	**3/3**
GW1-1	AF	N/A	N/A	N/A	N/A	F			
GW1-2	AF	N/A	N/A	N/A	N/A	F			
GW1-3	AF	N/A	N/A	N/A	N/A	F			
Site	**AF**	**N/A**	**N/A**	**N/A**	**N/A**	**F**	**N/A**	**N/A**	**0/3**
GW2-1	AF	R	98	-4.2	10.9	A			
GW2-2	AF	R	114.3	-20.8	16.2	A			
GW2-3	AF	R	158.7	-3.7	9	C			
Site	**AF**	**R**	**123.4**	**-10.6**	**53.7**	**B**	**53.7**	**6.34**	**3/3**
GW3-1	AF	N/A	N/A	N/A	N/A	F			
GW3-2	AF	N/A	N/A	N/A	N/A	F			

GW3-3	AF	N/A	N/A	N/A	N/A	F			
Site	**AF**	**N/A**	**N/A**	**N/A**	**N/A**	**F**	**N/A**	**N/A**	**0/3**
GW4-1	AF	R	272.7	-5.7	3.8	A			
GW4-2	AF	R	251.1	-4.6	4.2	A			
GW4-3	AF	N	333.8	55.6	11.5	B			
Site	**AF**	**N**	**N/A**	**N/A**		**B**	**N/A**	**N/A**	**3/3**
GW5-1	AF	N	4.7	61.2	9.2	B			
GW5-2	AF	N	18.7	61.1	11.2	B			
GW5-3	AF	N	353.6	67.3	3.4	B			
Site	**AF**	**N**	**6.6**	**63.6**	**10.1**	**B**	**10.1**	**151.32**	**3/3**
GW6-1	AF	N	114.8	46.5	7.6	A			
GW6-2	AF	N	280.2	52	14.1	C			
GW6-3	AF	N	115.4	38.8	6	A			
Site	**AF**	**N**	**125.5**	**67.5**	**91.4**	**B**	**91.4**	**2.92**	**3/3**
GW7-1	AF	N	25.2	41.6	6.1	A			
GW7-2	AF	N	48.6	44.4	8.9	A			
GW7-3	AF	N	21.7	47.5	8.7	A			
Site	**AF**	**N**	**31.9**	**45.1**	**16.5**	**A**	**16.5**	**56.7**	**3/3**
GW8-1	AF	N	339.7	63.8	12.6	B			
GW8-2	AF	N	0.3	56.1	9.6	A			
GW8-3	AF	N	353.9	68.2	11.8	B			

Site	**AF**	**N**	**351.9**	**63**	**12**	**B**	**12**	**106.25**	**3/3**
GW9-1	AF	N	130.7	49.6	15.4	C			
GW9-2	AF	N	331.6	67.4	9	C			
GW9-3	AF	N	46.9	31.6	13.6	C			
Site	**AF**	**N**	**61.9**	**64.5**	**77.4**	**C**	**77.4**	**3.62**	**3/3**
GW10-1	AF	N/A	N/A	N/A	N/A	F			
GW10-2	AF	N/A	N/A	N/A	N/A	F			
GW10-3	AF	N/A	N/A	N/A	N/A	F			
Site	**AF**	**N/A**	**N/A**	**N/A**	**N/A**	**F**	**N/A**	**N/A**	**0/3**
GW11-1	AF	N/A	N/A	N/A	N/A	F			
GW11-2	AF	N/A	N/A	N/A	N/A	F			
GW11-3	AF	N/A	N/A	N/A	N/A	F			
Site	**AF**	**N/A**	**N/A**	**N/A**	**N/A**	**F**	**N/A**	**N/A**	**0/3**
GW12-1	AF	N/A	N/A	N/A	N/A	F			
GW12-2	AF	N/A	N/A	N/A	N/A	F			
GW12-3	AF	N/A	N/A	N/A	N/A	F			
Site	**AF**	**N/A**	**N/A**	**N/A**	**N/A**	**F**	**N/A**	**N/A**	**0/3**
GW13-1	AF	N/A	N/A	N/A	N/A	F			
GW13-2	AF	N/A	N/A	N/A	N/A	F			
GW13-3	AF	N/A	N/A	N/A	N/A	F			
Site	**AF**	**N/A**	**N/A**	**N/A**	**N/A**	**F**	**N/A**	**N/A**	**0/3**

Overall	**AF**								**24/42**

Table 2 Site Mean Directions – ChRM's for Greasewood (GW) location

Sample Name	**Demag**	**Polarity**	**Declination**	**Inclination**	**MAD**	**Rank**	**Alpha 95**	**K(Site)**	**N/No**
HMW1-1	AF	N	352.4	55	7.6	A			
HMW1-2	AF	N	355.8	46.6	4.9	A			
HMW1-3	AF	N	354.9	46.5	6.6	C			
Site	**AF**	**N**	**354.5**	**49.4**	**7.7**	**B**	**7.7**	**260.28**	**3/3**
HMW2-1	AF	N	6.2	58.8	10	C			
HMW2-2	AF	N	303.8	62.7	10	D			
HMW2-3	AF	N	312.4	53.6	9.7	D			
Site	**AF**	**N**	**326.8**	**61.3**	**27.3**	**D**	**27.3**	**21.4**	**3/3**
HMW3-1	AF	N	341.6	73.6	8.2	B			
HMW3-2	AF	N	330.1	40.1	6.8	A			
HMW3-3	AF	N	356.4	72.6	7.5	A			
Site	**AF**	**N**	**338.3**	**62.7**	**31.2**	**B**	**31.2**	**16.64**	**3/3**
Overall	**AF**	**N**							**9/9**

Table 3 Site Mean Directions – ChRM's for Hart Mine Wash (HMW) location

Sample Name	Demag	Polarity	Declination	Inclination	MAD	Rank	Alpha 95	K(Site)	N/No
LCWBC2-1	AF	R	140.8	-23	12.2	B			
LCWBC2-2	AF	R	136.7	-26.5	5.9	B			
LCWBC2-3	AF	R	135.3	-12.9	14.3	C			
Site	**AF**	**R**	**137.5**	**-20.8**	**11.6**	**B**	**11.6**	**114.88**	**3/3**
LCWBC3-1	AF	N	171.6	58.3	10.6	A			
LCWBC3-2	AF	N	45.9	57.8	6.6	D			
LCWBC3-3	AF	N	204.9	49.2	5.5	A			
Site	**AF**	**N**	**166.1**	**72.7**	**65.2**	**C**	**65.2**	**4.65**	**3/3**
LCWBC4-1	AF	R	124.7	-26.9	2.1	B			
LCWBC4-2	AF	R	130.9	-32.8	0.9	B			
LCWBC4-3	AF	R	124.7	-38.1	0.8	B			
Site	**AF**	**R**	**126.8**	**-32.7**	**9.7**	**B**	**9.7**	**163.99**	**3/3**
Overall	**AF**								**9/9**

Table 4 Site Mean Directions – ChRM's for Bouse Incision (LCWBC) location

Sample Name	Demag	Polarity	Declination	Inclination	MAD	Rank	Alpha 95	K(Site)	N/No
LCWSW1-1	AF	N/A	N/A	N/A	N/A	F			
LCWSW1-2	AF	R	189.9	-34.6	19.6	C			
LCWSW1-3	AF	N/A	N/A	N/A	N/A	F			
Site	**AF**	**R**	**N/A**	**N/A**	**N/A**	**D**	**N/A**	**N/A**	**1/3**
LCWSW2-1	AF	R	165.2	-47.4	3.7	B			
LCWSW2-2	AF	R	171	-38.5	3.2	B			
LCWSW2-3	AF	R	177.8	-44	4.8	B			
Site	**AF**	**R**	**171.5**	**-43.4**	**9.7**	**B**	**9.7**	**162.05**	**3/3**
LCWSW3-1	AF	R	165.1	-38.1	4.3	B			
LCWSW3-2	AF	R	176.9	-38	1.2	A			
LCWSW3-3	AF	R	161.8	-40.8	1.5	A			
Site	**AF**	**R**	**168**	**-39.1**	**9.7**	**A**	**9.7**	**162.38**	**3/3**
Overall	**AF**								**7/9**

Table 5 Site Mean Directions – ChRM's for Lost Cabin Beds (LCWSW) location

Rock Magnetic Analysis

Curie Temperature Analysis

Curie temperature analysis was performed in this study to gain insight into the magnetic carrier of these different samples. Curie temperature analysis was done on multiple sites and locations and yielded numerous different results. Site RM1-2 has a relatively moderate magnetic susceptibility but has a stable heating curve between 0°C - 450°C. The heating curve significantly drops off between 570°C - 580°C. Site RM3-2 and RM3-3 magnetic susceptibility is significantly lower than RM1-2. Both heating curves are very unstable but there does seem to be a gradual decrease between 550°C - 580°C **(Figure 11).**

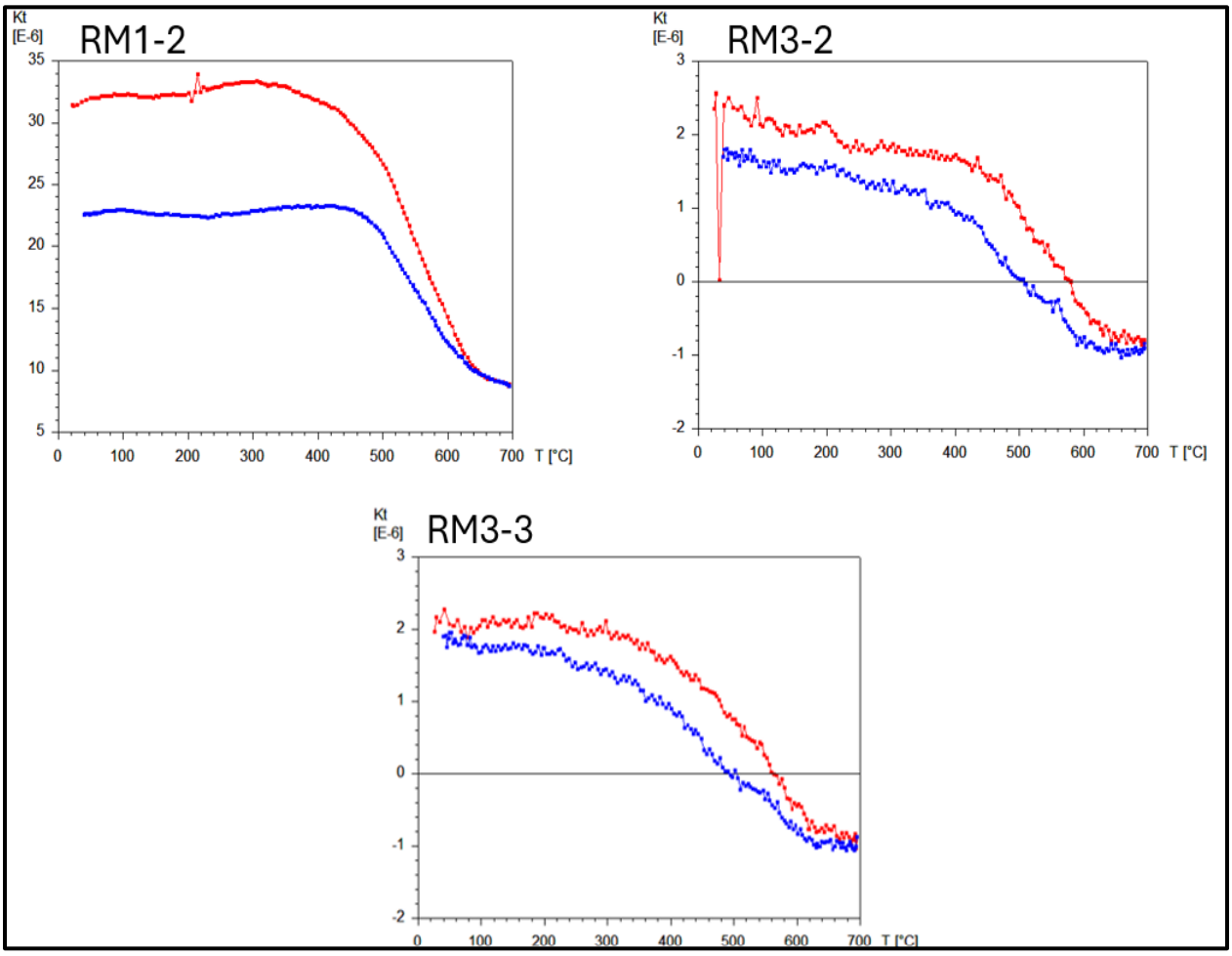


Figure 11: Thermomagnetic curves displaying all the Roberts Mesa samples that were run. The y-axis represents the magnetic moment of the sample in kilo Tesla and the x-axis represents the overall temperature of the sample in degrees Celsius.

Site GW0-3 magnetic susceptibility peaks around 300 - 350°C and begins a gradual decline until a significant drop is observed between 570°C - 580°C. It was also observed that the heating curve and cooling curve deviate from each other. Site GW5-1's heating curve seems to be relatively stable between 0°C - 450°C and then starts to drop around ~550°C until significantly dropping between 570 - 580°C. Site GW13-2 is very similar to site GW0-3 where there the heating curve is relatively stable between 0°C - 450°C and then significantly dropping off between 570°C - 580°C. Site GW13-2's magnetic susceptibility is a lot lower than the previous Greasewood samples run but still has a heating curve relatively stable between 0°C - 450°C and then significantly drops off between 570°C - 580°C **(Figure 12).**

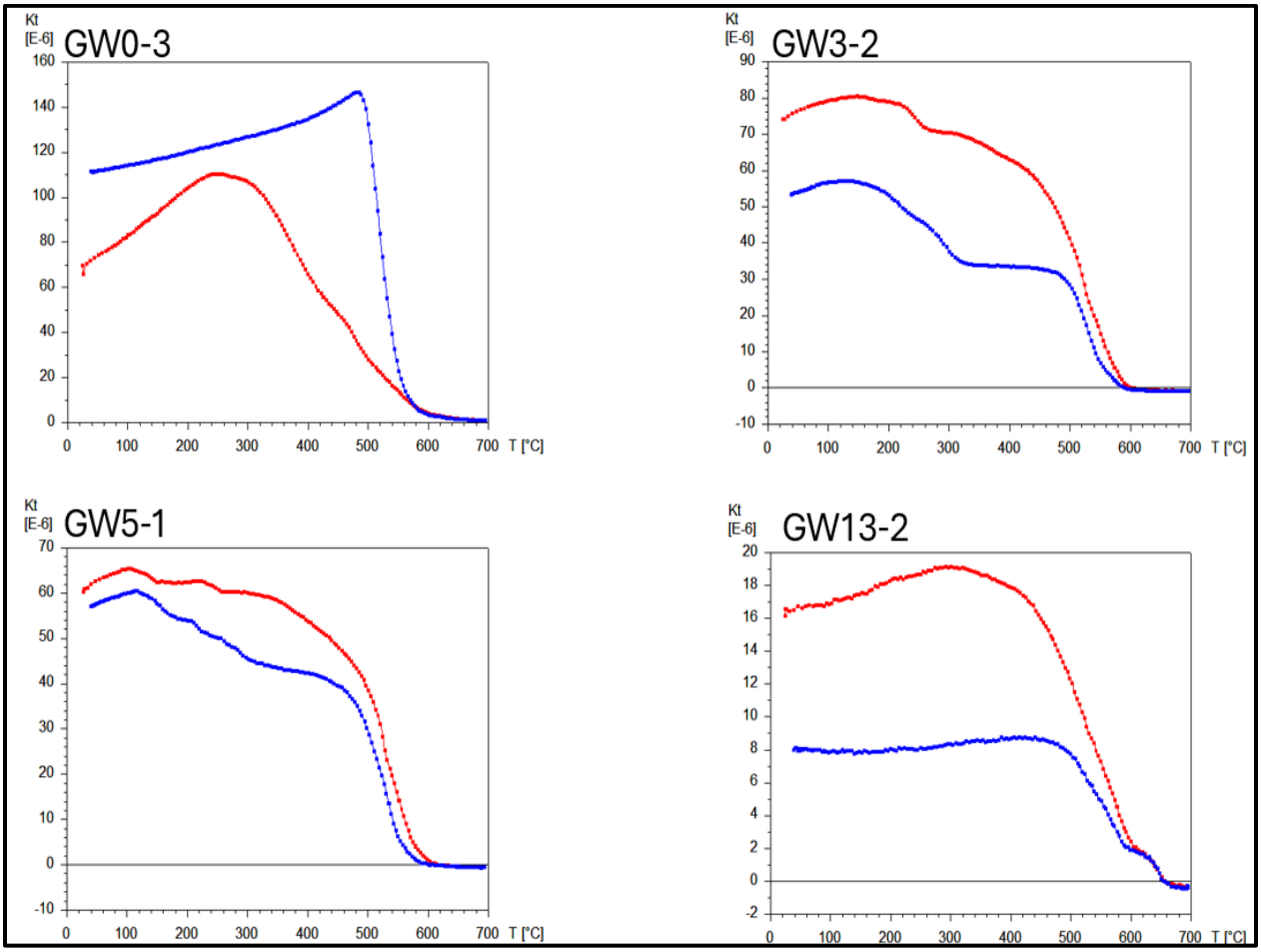


Figure 12: Thermomagnetic curves displaying all the Greasewood samples that were run. The y-axis represents the magnetic moment of the sample in kilo Tesla and the x-axis represents the overall temperature of the sample in degrees Celsius.

Two samples of each site were run on the samples LCWSW1-2 and HMW2-1. Site HMW2-1 yielded very little magnetic susceptibility consistent with Sangers (2023) HMW samples (**Figure 13).** Site LCWSW1-2 has a relatively high magnetic susceptibility and peaks around 300°C - 350°C and is relatively stable between 0°C - 450°C. The heating curve significantly drops off around 565°C - 580°C **(Figure 14).**

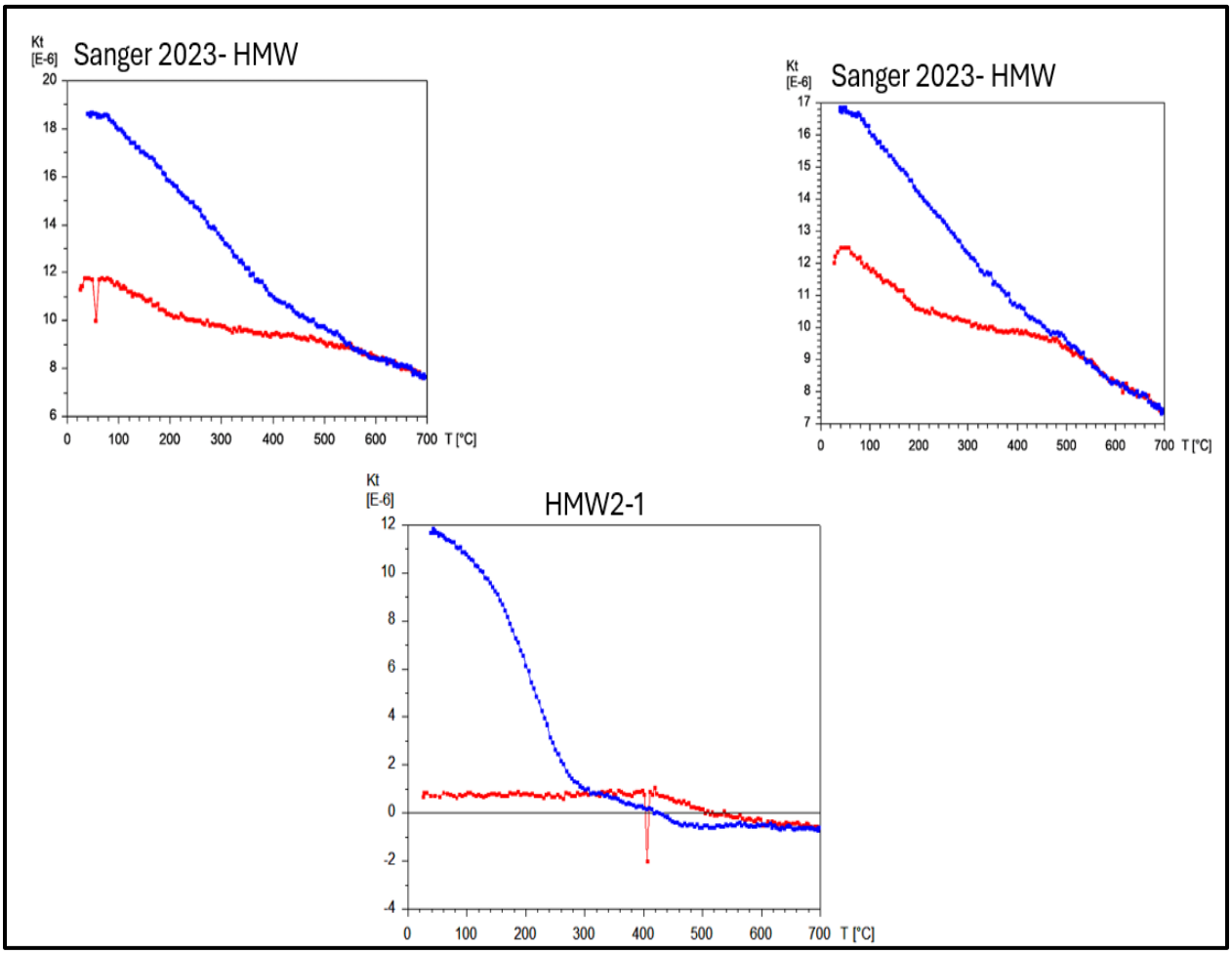


Figure 13: Thermomagnetic curves on the top are run by Sanger (2023) for HMW and the one on the bottom was run for this study. The y-axis represents the magnetic moment of the sample in kilo Tesla and the x-axis represents the overall temperature of the sample in

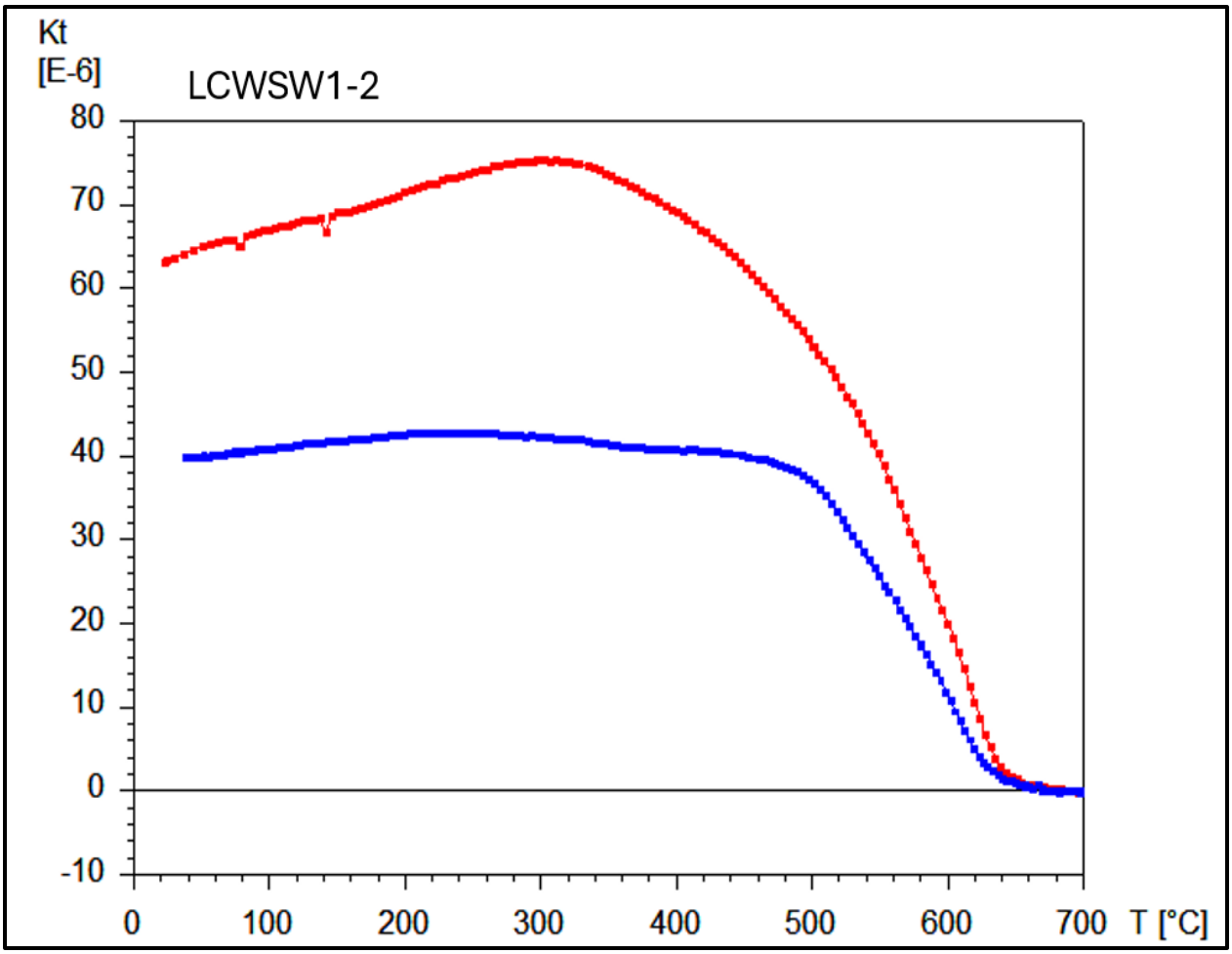


Figure 14: Thermomagnetic curves displaying the Lost Cabin Wash sample that was run. The y-axis represents the magnetic moment of the sample in kilo Tesla and the x-axis represents the overall temperature of the sample in degrees Celsius.

DISCUSSION

Magnetostratigraphy

Principal component analysis (PCA) was performed on all samples (graded A-C, some D) within this study to identify a ChRM that was representative of the magnetic polarity when these samples were deposited. All of the samples from this study are interpreted to have a primary detrital remanent magnetization (DRM), held in magnetite and titano-magnetite. Despite the lack of field tests to determine primary magnetization (all beds are near horizontal), all the rocks in this study fall within expected inclinations for Miocene-Pliocene aged sediments in this area. The Global Paleomagnetic Database (GPDMD.net) shows studies on Pliocene non-marine sediments in California with inclinations between 50-65° (Albright, 1999). Spatially and temporally, these are the closest studies to our study area. The lack of heating (by burial or other factors) beyond the unblocking temperature of the magnetizations and no known shock events (bolide impacts) also support the primary DRM interpretation of the magnetization. Little to no diagenetic alteration has been observed in these rocks. In addition, the rock magnetic tests agree with these interpretations, as magnetite and/or titanomagnetite are the only magnetic carriers present.

Roberts Mesa

Roberts Mesa samples yielded normal polarity values with the exception of 2 samples within two different sites (RM4-3 & RM5-1) as seen in **Figure 15.** These negative inclination values are very shallow and would not pass a reversal test, but they still received an A and B quality when grading these orthogonal projections due to linear decay of the magnetization with little noise. Since there is only one sample out of three samples for each site that hold the negative inclination values, all sites at Roberts Mesa are interpreted to be within a normal polarity chron. However, since these negative inclination values receive an A and B letter grade, we cannot ignore these values and interpret them as

either recording a potential magnetic excursion within the C3An.2n normal polarity chron, or sample orientation error.

Two samples were collected in May of 2024 from Roberts Mesa for U-Pb dating. Ash RC240506-RM-2 yielded a date of 6.54 ± 0.09 Ma and falls between samples RM10 and RM11 while ash RC240506-RM-5 yielded a date of 6.46 ± 0.15 Ma and falls between RM12 and RM13 (personal communication, Ryan Crow). These ash dates were used as anchor points within Roberts Mesa which helped us interpret that the majority of the Roberts Mesa section lies within the C3An.2n normal polarity chron **(Figure 15).**

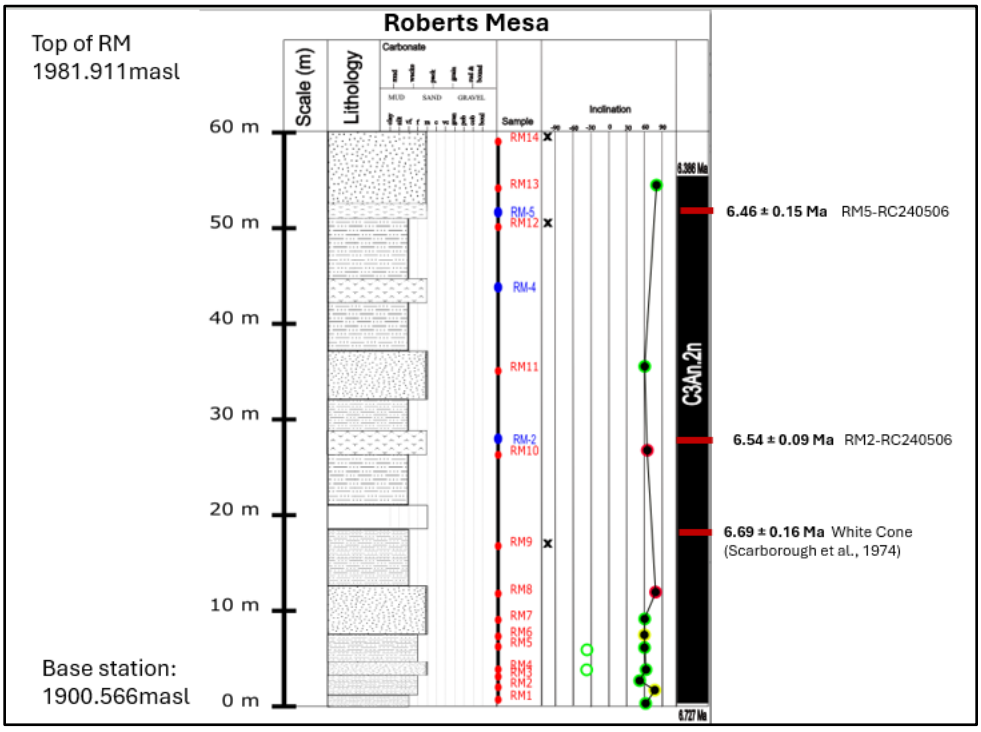


Figure 15 Stratigraphic column showing sample location in Roberts Mesa including the magnetostratigraphy (red) and the preliminary ash dates (blue). Black circles represent reverse polarity samples and black circles represent normal polarity samples. The green circle represents anything that was graded an A or B. Yellow circles represent anything that was graded a C and the red circles represent D graded samples.

Greasewood

Greasewood samples also yielded normal polarity values with the exception of one site where all three samples yielded reversed polarity values (GW2) and one site (GW4) that yielded two out of three reverse polarity values as seen in **Figure 16**. Again, these negative

inclination values are very shallow and would not pass a reversal test but are interpreted to be an excursion within the C3An.2n normal polarity chron.

The two ash dates from Greasewood were used as anchoring points to the GPTS. Low in the section Dallege et al. (2003) identified the Blacktail Creek ash dated at 6.62 ± 0.05 Ma. Ash RC240507-GR3 is a preliminary ash date sampled in May 2024 and yielded a date of 6.42 ± 0.08 Ma. (personal communication, Ryan Crow). These two ash dates help better constrain the hypothesis that the majority of the Greasewood outcrop lies within the C3An.2n normal polarity chron (**Figure 16).**

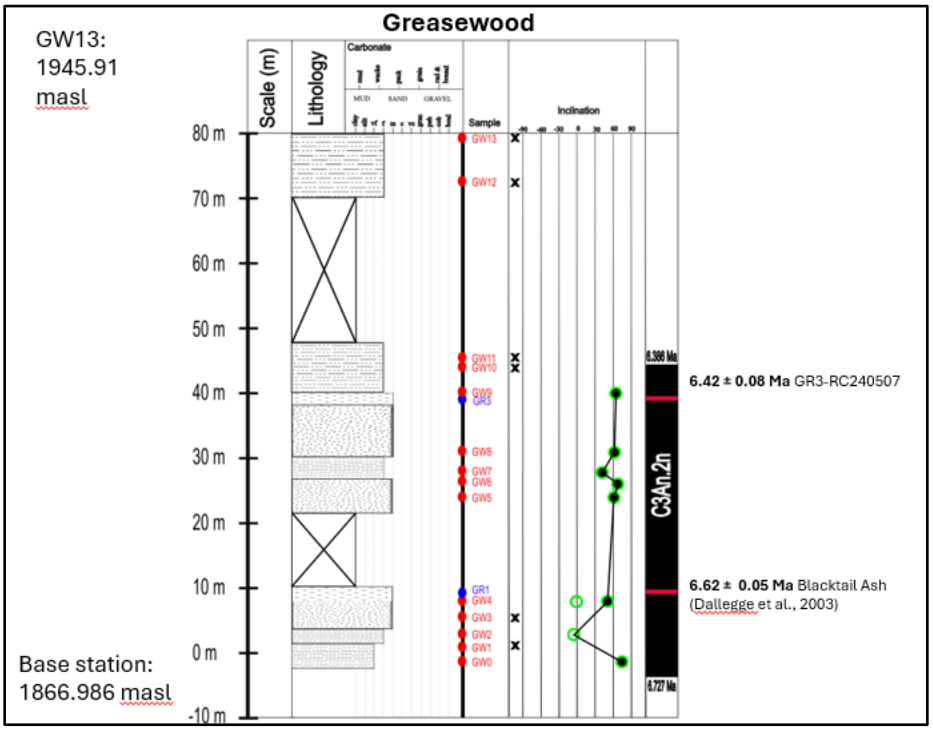


Figure 16 Stratigraphic column showing sample location in Greasewood Canyon including the magnetostratigraphy (red) and the preliminary ash dates (blue). Black circles represent reverse polarity samples and black circles represent normal polarity samples. The green circle represents anything that was graded an A or B. Yellow circles represent anything that was graded a C and the red circles represent D graded samples.

Hart Mine Wash

Samples within this study from Hart Mine Wash revealed all normal polarity values. Magnetostratigraphic results from Sanger (2023) found majority normal polarity results below the 4.8 Ma Hart Mine Wash ash but found two reverse polarity sites directly below the HMW ash. Additional samples were collected by Crow below (HMW 1) and above

(HMW 2 & HMW 3) the ash to constrain the potential reversal **(Figure 5).** This was unsuccessful because all the samples that were run within this study yielded normal polarity inclinations. However, this does not discount Sanger's (2023) magnetostratigraphic data within HMW therefore further sampling is needed above this HMW ash.

Lost Cabin Wash

LCWBC (Lost Cabin Wash Bouse Cove)

Site LCWBC is described as a Bouse fluvial incision site and exhibits an unconformable contact between the Bouse Formation and the underlying Lost Cabin beds. **(Figure 17)**. Schwing's (2019) magnetostratigraphic data yielded 4 samples within the filled channel that exhibit negative inclinations. Additional samples within the LCWBC site were processed in this study and yielded two additional negative inclination sites (LCWBC2 & LCWBC4) and one site (LCWBC3) with positive inclinations. This suggests that a reverse polarity subchron within this incision site exists, but it cannot be exactly placed within the GPTS due to the presence of the unconformity. However, it is likely that this site represents the C3n.3r reverse polarity subchron because it is thought that the Colorado River had reached Cottonwood and Mohave Valley by 4.7 to 5.24 Ma (Schwing 2019; Crow et al., 2021).

LCWSW (Lost Cabin Wash Southwest)

Sites LCWSW1 through LCWSW3 were additional pre-Bouse samples taken by Schwing (2019) from the Lost Cabin beds that were run and analyzed as part of this study. These sites revealed all negative inclination values. Schwing's (2019) magnetostratigraphic results within the Lost Cabin beds yielded majority reverse polarity samples which he correlated to the reverse C3r (Gilbert) subchron. Our results within this study further constrain the pre Bouse Lost Cabin beds to be deposited within this reverse C3r (Gilbert) subchron.

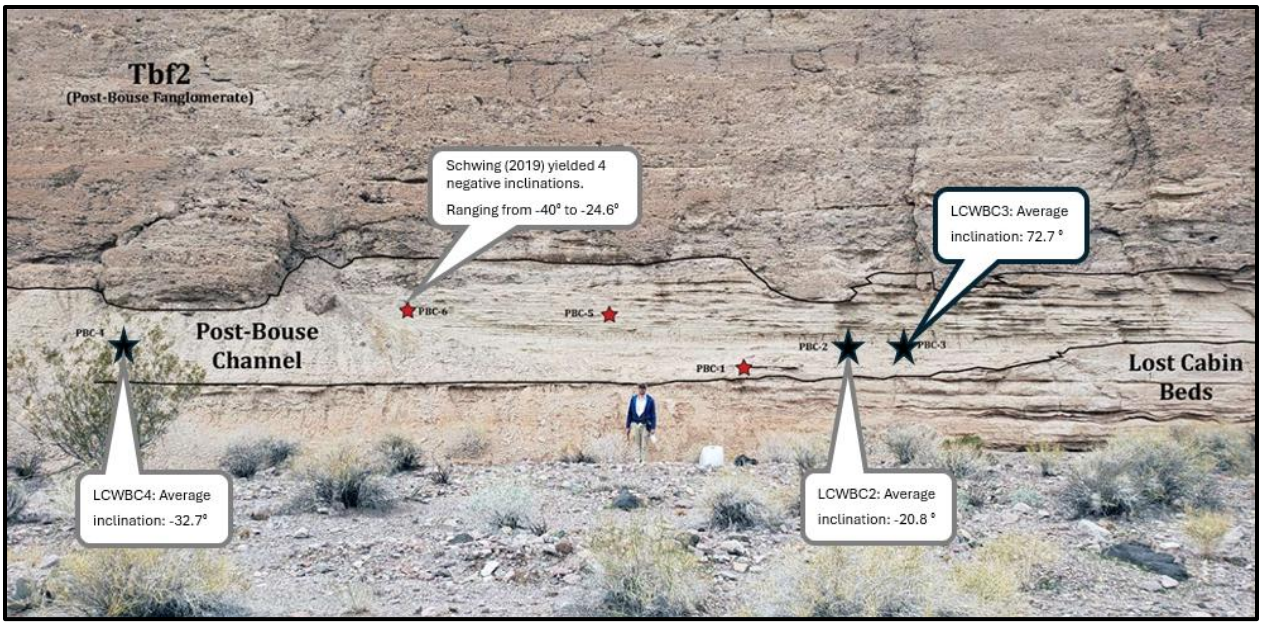


Figure 17: Modified from Schwing (2019) shows the Bouse Fluvial incision site with black stars indicating sites that were run in this study and red stars representing samples that were taken by Schwing.

Curie Temperature Analysis

Curie temperature analysis was done on samples from each location. All samples yielded a difference in magnetic susceptibility but had a consistent range in Curie points (565°C - 580°C). These results are consistent with the Curie point of magnetite, which has a curie point of ~580°C. The differing results where some of the Curie points are lower than ~580°C is attributed to the presence of titanomagnetite. An increase of titanium within magnetite causes the Curie point to be lower than ~580°C. The curie temperature decreases with increasing titanium because of the replacement of iron with titanium disrupts the exchange interactions that stabilize the magnetic order (personal communication, Michael Petronis & Luke Romero). In summary, the majority of the samples within all the samples are consistent with magnetite and varying compositions (high to low) of Ti-titanomagnetite.

Poor Data Results

Out of 108 samples 29 were graded as F quality due to no or non-linear decay of the magnetic directions. We attribute these data to possible disturbance of magnetic grains

during sampling, or non-uniformity of magnetic grains during deposition. Field conditions were not ideal for sampling since recent precipitation made the samples very friable. When extracting these samples, it is possible that these samples could have been distorted due to handling which would disrupt the sediments within the rock. Originally, we hypothesized that the larger grain sized samples could have been less stable due to the potential increase in multi-domain magnetite but there seems to be no support for this hypothesis, since some coarser grained samples yielded higher graded data. Most likely, there is a large amount of multi-domain magnetite within the majority of the samples which can obscure the primary magnetization at low mT steps.

Within the A/B/C/D graded samples, the majority of the MAD angles are very high (>15) which is not statistically valid. We attribute these high MAD angles and low K-values to the steeply inclined magnetizations, which yield a wide deviation of declination angles which skew the statistics. However, within most of the sites the inclination values within each sample correlate well and the magnetization shows linear decay, therefore meriting high grades despite the high MAD angles.

Sedimentation Rates

The majority of the data are interpreted to fall within the normal polarity C3An.2n subchron in Greasewood and Roberts Mesa, which allows us to make some estimates for sedimentation rates in the Bidahochi basin. These rates do not represent actual sedimentation rates since our sampling does not span the entire chron, but instead provide estimates based on the preliminary ash dates and the length of the C3An.2n chron. Using the preliminary ash dates and the length of the C3An.2n chron at the Greasewood section we calculated sedimentation rates ranging from 0.132mm/yr to 0.150mm/yr. The same method was used at the Roberts Mesa section where we calculated rates ranging from 0.175mm/yr to 0.313mm/yr.

Average depositional rates in lakes is about 1mm/yr, although environment of deposition and age of the sediments sampled yields a wide range of rates (Sadler, 1981).

Lake Tanganyika, a deep rift-lake in Eastern Africa, has a low sedimentation rate of ~0.3mm/yr, with sediments mostly formed from settling organics and planktonic fallout, and clastic muds from local run-off. These sedimentation rates calculated from paleo Lake Hopi ranging from 0.132mm/yr to 0.313mm/yr are still likely lower than would be expected but fall within the range of lake systems (Sadler, 1981). In comparison, previous interpretations (Sanger, 2023; Andy Cohen, personal communication) of the Bouse Formation at Mesquite Mountain in the Blythe basin imply high sedimentation rates. The Mesquite Mountain section is a 50m thick interval of Bouse that is entirely within one normal polarity interval of the Gilbert Chron but is not bracketed by ash dates and therefore cannot be narrowed down further.

Using a basin sill estimation of 2285 m, an estimated size of 70,000 km^2 for (Douglass et al., 2020) the paleo-basin, and an average basin floor depth of 1900 m, we calculated how long it would take to fill the basin using our newly proposed sedimentation rates. Using the lower end of our newly proposed sedimentation rate (0.132 mm/yr) we calculated it would have taken approximately ~2.9 Ma years to fill the entire Bidahochi basin assuming uniform deposition throughout the basin. On the higher end of our newly proposed sedimentation rate (0.313mm/yr) we calculated it would have taken approximately ~1.2 Ma to fill the entire Bidahochi basin assuming uniform deposition throughout the basin.

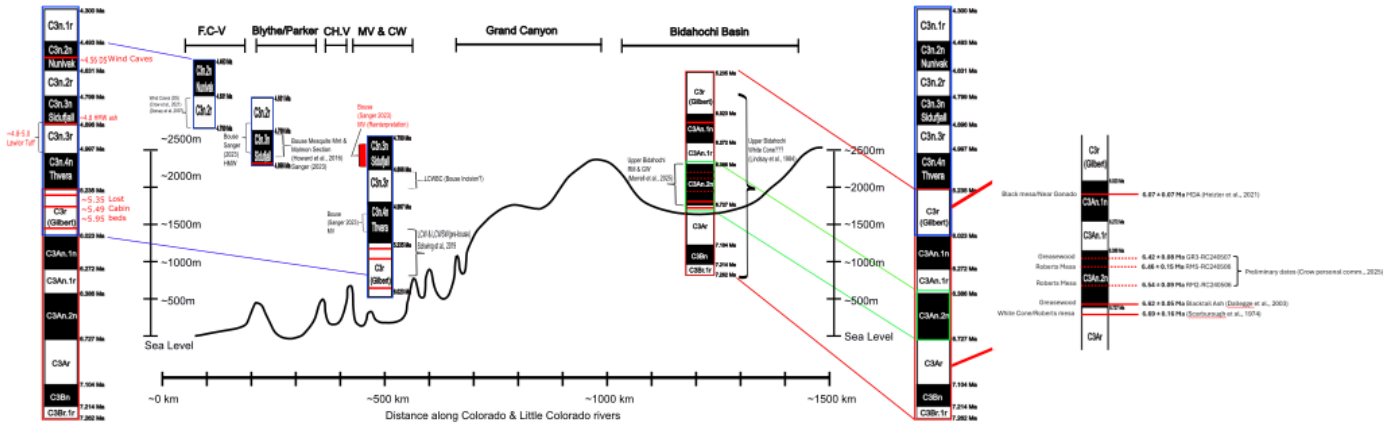


Figure 18 Compilation of Magnetostratigraphic Data within the Bidahochi Basin & the Lower Colorado River Corridor. Red callouts represent Lindsay et al. (1984) interpretation of White Cone. Green callout represents this studies interpretation of the upper member of the Bidahochi at Roberts Mesa and Greasewood. Blue callouts represent the chrons found within the LOCO. Important ash dates are listed within the Bidahochi and the LOCO. Red bracket is representative of a reinterpretation of Sanger (2023). Black brackets are interpretations of magnetostratigraphic data done throughout the Bidahochi and the LOCO.

Big Picture

Figure 18 shows a compilation of the magnetostratigraphic work done within the Bidahochi basin and the lower Colorado river corridor. The Bidahochi basin highlighted in red is the interpreted section of White cone done by Lindsay (1984) and highlighted in green is our interpreted section of Roberts Mesa and Greasewood where we interpreted the majority of the section to lie within the normal C3An.2n subchron.

Schwing's (2019) study done on the Lost Cabin beds within Cottonwood Valley interpreted the majority of the section to be within the reverse C3r subchron capturing a reversal into the normal polarity Thvera subchron. This study further corroborated that result as three sites ran within this study (LCWSW) that also yielded negative inclination values in the Lost Cabin beds. Sanger (2023) found majority normal polarity inclinations within Mohave Valley in which he interpreted to be the Thvera subchron. There are no absolute dates within the sampled magnetostratigraphic section in Mohave Valley, so further work is needed there to confirm whether this section lies within the normal Thvera or Sidufjall subchron. The incised Bouse channel found within the Lost Cabin beds (LCWBC) yielded negative inclination results which are interpreted to be within the negative C3n.3r subchron. This interpretation infers the possibility that the normal polarity Bouse deposits downstream (including Sanger's Mohave section) lie within the Sidufjall subchron.

Downstream in Park Moabi basin, Sanger's (2023) Mesquite Mountain data supports work done on the Malmon section (Howard et al., 2016) that most of the section is normal polarity and likely lies within the normal Sidufjall subchron.

Within the Blythe basin Hart Mine Wash magnetostratigraphy data (Sanger, 2019) was interpreted using the 4.8 Ma Hart Mine Wash ash and the 4.8 to 5.0 Ma Lawlor tuff found high in the Bouse. This section is interpreted to lie within the normal Sidufjall subchron further constrained by the samples run within this study showing positive inclination values. Further work is needed to confirm the reversal from the normal Sidufjall subchron into the reverse C3n.2r subchron found by Sanger (2023) near the 4.8 Hart Mine Wash ash.

Within the southernmost Fish-Creek Vallecito basin Crow et al. (2021) report a maximum depositional detrital sanidine age within the upper part of Wind Caves member of 4.56 ± 0.04 which lies within the normal Nunivak subchron. The first arriving Colorado River sands are lower stratigraphically in a reversed polarity interval interpreted by Crow et al. (2021) to be the C3n.2r. Previous magnetostratigraphic data within this same basin reports the wind caves member to be within reverse C3r gilbert subchron which is much older than the DS date. This data is hung on a ~2 Ma year old ash and is now a questioned interpretation due to this newly discovered detrital sanidine age (Crow et al., 2021).

CONCLUSIONS

The magnetostratigraphy of the upper Bidahochi Formation, coupled with the newly sampled preliminary ash dates from Roberts Mesa and Greasewood Canyon, suggest that these two sample sites lie within the normal C3An.2n subchron. This suggests that most of the upper member of the Bidahochi was deposited between 6.727 Ma and 6.386 Ma. Using our magnetostratigraphic points and preliminary ash data, we suggest new sedimentation rates within the upper member of the Bidahochi that range from 0.132 mm/yr to 0.313 mm/yr. We also suggest that we have captured a potential excursion at both sites within the C3An.2n but further work is needed to confirm this. Due to poor data quality within the top ~40m of section within Greasewood and our large sampling interval, we cannot confirm whether the entirety of Greasewood lies within normal C3An.2n subchron.

This data does put the magnetostratigraphy work done at White Cone by Lindsey et al., (1984) in question where they interpreted multiple subchrons within the Gilbert chron. Our sites, Greasewood and Roberts Mesa, have thicker sections of the upper Bidahochi that were not present at White Cone, and it is unlikely that this data at White Cone is representative of the entire upper Bidahochi member. However, our sample density with Greasewood and Roberts Mesa was on average one site every ~8m (compared to Lindsays (1984) average of one site per 3.18m), and the upper sections of Greasewood yielded no results. Additional sampling of the upper member of the Bidahochi at White Cone and the upper sections of Greasewood should be conducted to confirm the hypothesis that the majority of the upper Bidahochi lies within the normal C3n.An subchron.

The magnetostratigraphy work done within this study at Hart Mine Wash reveals ambiguous results when compared to Sangers (2023) work. Further sampling at closely spaced intervals below and above the 4.8 Ma Hart Mine Wash ash is needed in order to confirm if there is a reversal present.

The magnetostratigraphy work done within the Lost Cabin beds further confirms Schwings (2019) hypothesis that the Lost Cabin beds lie within the reverse Gilbert (C3r) subchron which supports the idea that the Colorado River arrived within Cottonwood and Mohave valleys during or after the normal Thvera (C3n.4n) subchron. The Bouse incision site (LCWBC) is unable to be assigned to a specific subchron due to the disconformity present, but it is most likely representative of the C3n.3r reverse polarity subchron which would support the findings that the Colorado River was deposited during or after the Thvera subchron. This interpretation means that the normal polarity Bouse deposits downstream of this location most likely lie within the Sidufjall subchron.

This study has constrained the timing of deposition in the upper Colorado River Bidahochi basin as well as further constraining the timing of arrival of pre-Colorado River and Colorado River sediments throughout the lower Colorado River corridor.

REFERENCES

Albright, L. B. III. (1999). Magnetostratigraphy and biochronology of the San Timoteo Badlands, southern California, with implications for local Pliocene–Pleistocene tectonic and depositional patterns. *Journal of Geophysical Research: Solid Earth, 104*(B1), 339–368. https://doi.org/10.1029/1998JB900020

Aslan, A., Karlstrom, K.E., Kirby, E., Heizler, M.T., Granger, D.E., Feathers, J.K., Hanson, P.R., and Mahan, S.A., 2019, Resolving time-space histories of Late Cenozoic bedrock incision along the Upper Colorado River, USA: Geomorphology, v. 347, p. 106855, doi:10.1016/j.geomorph.2019.106855.

Beard, L. S., Karlstrom, K. E., Young, R. A., & Billingsley, G. H. (Eds.). (2011). *CRevolution 2—Origin and evolution of the Colorado River system: Workshop abstracts* (U.S. Geological Survey Open-File Report 2011-1210, 300 p.). U.S. Geological Survey.

Bennett, S. E. K., Darin, M., Dorsey, R. J., Thompson, L., Umhoefer, P. J., & Oskin, M. E. (2016, April 16). Animated tectonic reconstruction of the Lower Colorado River region: Implications for late Miocene to present deformation. *2016 Desert Symposium*.

Buising, A. V. (1990). The Bouse Formation and bracketing units, southeastern California and western Arizona: Implications for the evolution of the Proto–Gulf of California and the lower Colorado River. *Journal of Geophysical Research: Solid Earth, 95*(B12), 20111–20132. https://doi.org/10.1029/JB095iB12p20111

Butler, R. F. (1992). *Paleomagnetism: Magnetic domains to geologic terranes*. Blackwell Scientific Publications.

Cohen, A., Cassidy, C., Crow, R., Bright, J., Crossey, L., Dorsey, R., Gootee, B., House, K., Howard, K., Karlstrom, K., & Pearthree, P. (2019). The Bouse Formation, a controversial Neogene archive of the evolving Colorado River: A scientific drilling workshop report (28 February–3 March 2019 – BlueWater Resort & Casino, Parker, AZ, USA). *Scientific Drilling, 26*, 59–67. https://doi.org/10.5194/sd-26-59-2019

Coney, P. J., & Harms, T. A. (1976). Cordilleran metamorphic core complexes: Cenozoic extensional relics of Mesozoic compression. *Geology, 4*(3), 105–110.

Crow, R. S., Howard, K. A., Beard, L. S., Pearthree, P. A., House, P. K., Karlstrom, K. E., Peters, L., McIntosh, W., Cassidy, C., Felger, T. J., & Block, D. (2019). Insights into post-Miocene uplift of the western margin of the Colorado Plateau from the stratigraphic record

of the lower Colorado River. *Geosphere, 15*(6), 1826–1845. https://doi.org/10.1130/GES02020.1

Crow, R., Karlstrom, K. E., Asmerom, Y., Schmandt, B., Polyak, V., & DuFrane, S. A. (2011). Shrinking of the Colorado Plateau via lithospheric mantle erosion: Evidence from Nd and Sr isotopes and geochronology of Neogene basalts. *Geology, 39*(1), 27–30. https://doi.org/10.1130/G31611.1 .

Crow R.S, J. Schwing, K.E. Karlstrom, M. Heizler, P.A. Pearthree, P.K. House, S. Dulin, S.U. Jänecke, M. Stelten, L.J. Crossey; (2021) Redefining the age of the lower Colorado River, southwestern United States. *Geology* 2; 49 (6): 635–640. doi: https://doi.org/10.1130/G48080.1

Crow, R., Gootee, B., House, K., Pearthree, P., Vazquez, J., Walkup, L., Brennan, K., Lidzbarski, M., Holm-Denoma, C., Croxen, F., & Bright, J. (2025, April). Depositional age of the Bouse Formation and early integration history of the lower Colorado River. In Abstracts from Proceedings: The 2025 Desert Symposium. Desert Studies Consortium.

Dallegge, T. A., Ort, M. H., & McIntosh, W. C. (2003). Mio-Pliocene chronostratigraphy, basin morphology and paleodrainage relations derived from the Bidahochi Formation, Hopi and Navajo Nations, northeastern Arizona. *The Mountain Geologist, 40*(2), 55–75.

Dickinson, W. R. (2011). Bidahochi paleogeography and incision of the Grand Canyon. In L. S. Beard, K. E. Karlstrom, R. A. Young, & G. H. Billingsley (Eds.), *CRevolution 2—Origin and evolution of the Colorado River system: Workshop abstracts* (pp. 81–87). U.S. Geological Survey Open-File Report 2011-1210.

Dickinson, W. R., & Snyder, W. S. (1979). Geometry of subducted slabs related to San Andreas transform. *The Journal of Geology, 87*(6), 609–627.

Dorsey, R. J., Housen, B. A., Janecke, S. U., Fanning, C. M., & Spears, A. L. F. (2011). Stratigraphic record of basin development within the San Andreas fault system: Late Cenozoic Fish Creek–Vallecito basin, southern California. *Geological Society of America Bulletin, 123*(5–6), 771–793.

Douglass, J. C. (1999). *Late Cenozoic landscape evolution study of the eastern Grand Canyon region* (Master's thesis). Northern Arizona University, Flagstaff, AZ.

Douglass, J. C. (2011). One Grand Canyon but four mechanisms—Was it antecedence, superimposition, overflow, or piracy? In L. S. Beard, K. E. Karlstrom, R. A. Young, & G. H. Billingsley (Eds.), *CRevolution 2—Origin and evolution of the Colorado River system: Workshop abstracts* (pp. 93–98). U.S. Geological Survey Open-File Report 2011-1210.

Douglass, J. C., Gootee, B. F., Dallegge, T., Jeong, A., Seong, Y. B., & Yu, B. Y. (2020). Evidence for the overflow origin of the Grand Canyon. *Geomorphology, 369*, 107361. https://doi.org/10.1016/j.geomorph.2020.107361

Faulds, J.E., Schreiber, B.C., Langenheim, V.E., Hinz, N.H., Shaw, T.H., Heizler, M.T., Perkins, M.E., El Tabakh, M., and Kunk, M.J., 2016, Paleogeographic implications of late Miocene lacustrine and nonmarine evaporite deposits in the Lake Mead region: Immediate precursors to the Colorado River: Geosphere , v. 12, p. 721–767, https://doi.org/10.1130/GES01143.1.

Fisher, R. A. (1953). Dispersion on a sphere. *Proceedings of the Royal Society of London. Series A. Mathematical and Physical Sciences, 217*(1130), 295–305.

Gardner, M. H., & Dorsey, R. J. (2021). Identification of seasonal varves in the lower Pliocene Bouse Formation, lower Colorado River Valley, and implications for Colorado Plateau uplift. *Geosphere, 17*(6), 1745–1761. https://doi.org/10.1130/GES02419.1

Hanna, G. D. (1926). Pliocene marine mollusks from the Colorado Desert region. *University of California Publications in Geological Sciences, 16*(11), 187–198.

Howard, K. A., Malmon, D. V., Hillhouse, J. W., Dorsey, R. J., Crow, R. S., & House, P. K. (2016). Magnetostratigraphic constraints on the Bouse Formation in the Blythe Basin: Existing evidence. In R. E. Reynolds (Ed.), *2016 Desert Symposium Field Guide and Proceedings* (pp. 97–100). California State University Desert Studies Center, Zzyzx, CA.

House, P.K., Pearthree, P.A., and Perkins, M.E., 2008, Stratigraphic evidence for the role of lake spillover in the inception of the lower Colorado River in southern Nevada and western Arizona, *in* Reheis, M., Hershler, R., and Miller, D. eds., Late Cenozoic Drainage History of the Southwestern Great Basin and Lower Colorado River Region: Geologic and Biotic Perspectives: Geological Society of America Special Paper 439, v. 80301, p. 335–353, doi:10.1130/2008.2439(15).

Karlstrom, K. E., Crow, R., Crossey, L. J., Coblentz, D., & Van Wijk, J. (2008). Model for tectonically driven incision of the younger than 6 Ma Grand Canyon. *Geology, 36*(11), 835–838. https://doi.org/10.1130/G25032A.1

Karlstrom, K. E., Young, R. A., Beard, L. S., Billingsley, G. H., House, P. K., Aslan, A., & Pederson, J. (2011). Summary report. In L. S. Beard, K. E. Karlstrom, R. A. Young, & G. H. Billingsley (Eds.), *CRevolution 2—Origin and evolution of the Colorado River system: Workshop abstracts* (pp. 3–16). U.S. Geological Survey Open-File Report 2011-1210.

Levander, A., Schmandt, B., Miller, M. S., Liu, K. H., Karlstrom, K. E., Crow, R., … & Humphreys, E. D. (2011). Continuing Colorado Plateau uplift by delamination-style convective lithospheric downwelling. *Nature, 472*(7344), 461–465. https://doi.org/10.1038/nature10001

Lindsay, E. H., Opdyke, N. D., & Johnson, N. M. (1984). Blancan-Hemphillian Land Mammal Ages and Late Cenozoic Mammal Dispersal Events. *Annual Review of Earth and Planetary Sciences, 12*, 445–488. https://doi.org/10.1146/annurev.ea.12.050184.002305

Love, J. J. (2007). Principal component analysis in paleomagnetism. In D. Gubbins & E. Herrero-Bervera (Eds.), *Encyclopedia of Geomagnetism and Paleomagnetism* (pp. 845–850). Springer.

Lucchitta, I. (1972). Early history of the Colorado River in the Basin and Range province. *Geological Society of America Bulletin, 83*(7), 1933–1948.

Lucchitta, I. (1984). Development of landscape in northwest Arizona: The country of plateaus and canyons. In T. L. Smiley, J. D. Nations, T. L. Péwé, & J. P. Schafer (Eds.), *Landscapes of Arizona: The geological story* (pp. 269–301). Lanham, MD: United Press of America.

Lucchitta, I. (1989). History of the Grand Canyon and of the Colorado River in Arizona. In J. P. Jenney & S. J. Reynolds (Eds.), *Geologic evolution of Arizona* (pp. 701–715). Arizona Geological Society Digest 17.

Lucchitta, I. (1990). History of the Grand Canyon and of the Colorado River in Arizona. In S. S. Beus & M. Morales (Eds.), *Grand Canyon geology* (pp. 311–332). New York, NY: Oxford University Press.

Malmon, D.V., Howard, K.A., and Hillhouse, J.W., 2011a, New observations of the Bouse Formation in Chemehuevi and Parker valleys, in Beard, L.S., Karlstrom, K.E., Young, R.A., and Billingsley, G.H., CREvolution 2—Origin and Evolution of the Colorado River System, Workshop Abstracts: U.S. Geological Survey Open-file Report 2011-1210, p.204–205, http://pubs.usgs.gov/of/2011/1210/.

Mavor, S. P., Bennett, S. E. K., Crow, R. S., Singleton, J. S., Langenheim, V., Stockli, D., Stelten, M., Brickey, T. A., Umhoefer, P. J., & Beard, L. S. (2023). Evolution of Miocene normal and dextral faulting in the lower Colorado River region near Blythe, California, USA. *Geosphere, 19*(5), 1180–1209. https://doi.org/10.1130/GES02608.1

McDougall, K. (2008). Late Neogene marine incursions and the ancestral Gulf of California. In M. C. Reheis, R. Hershler, & D. M. Miller (Eds.), *Late Cenozoic drainage history of the

southwestern Great Basin and lower Colorado River region: Geologic and biologic perspectives* (Vol. 439, pp. 355–373). Geological Society of America. https://doi.org/10.1130/2008.2439(16)

McDougall, K., & Martínez, A. Y. M. (2014). Evidence for a marine incursion along the lower Colorado River. *Geosphere, 10*(4), 842–869. https://doi.org/10.1130/GES00975.1

McDougall, K., O'Connell, B., Dorsey, R. J., & Miranda Martínez, A. Y. (2017). Punctuated sediment discharge during early Pliocene birth of the Colorado River: Evidence from regional stratigraphy, sedimentology, and paleontology. *Sedimentary Geology, 363*, 16–34. https://doi.org/10.1016/j.sedgeo.2017.09.018

Morgan, G. S., & White, R. S. Jr. (2005). Miocene and Pliocene vertebrates from Arizona. In R. S. White Jr. (Ed.), *Vertebrate Paleontology in Arizona: Bulletin*, 29, 114.

Moucha, R., Forte, A. M., Mitrovica, J. X., Rowley, D. B., Quéré, S., Simmons, N. A., & Grand, S. P. (2008). Dynamic topography and long-term sea-level variations: There is no such thing as a stable continental platform. *Earth and Planetary Science Letters, 271*(1–4), 101–108. https://doi.org/10.1016/j.epsl.2008.03.056

Ogg, J. G. (2020). Geomagnetic polarity time scale. In F. M. Gradstein, J. G. Ogg, M. D. Schmitz, & G. M. Ogg (Eds.), *Geologic time scale 2020* (Chapter 5). Elsevier. https://doi.org/10.1016/B978-0-12-824360-2.00005-X

O'Connell, B., Dorsey, R. J., & Humphreys, E. D. (2017). Tidal rhythmites in the southern Bouse Formation as evidence for post-Miocene uplift of the lower Colorado River corridor. *Geology, 45*(2), 99–102. https://doi.org/10.1130/G38608.1

Pearthree, P. A., & House, P. K. (2014). Paleogeomorphology and evolution of the early Colorado River inferred from relationships in Mohave and Cottonwood valleys, Arizona, California, and Nevada. *Geosphere, 10*(6), 1139–1160. https://doi.org/10.1130/GES00988.1

Pelletier, J. D. (2010). Numerical modeling of the late Cenozoic geomorphic evolution of Grand Canyon, Arizona. *Geological Society of America Bulletin, 122*(3–4), 595–608. https://doi.org/10.1130/B26403.1

Repenning, C. A., & Irwin, J. H. (1954). Bidahochi Formation of Arizona and New Mexico. *American Association of Petroleum Geologists Bulletin, 38*, 1821–1826.

Roberts, G. G., White, N. J., Martin-Brandis, G. L., & Crosby, A. G. (2012). An uplift history of the Colorado Plateau and its surroundings from inverse modeling of longitudinal river profiles. *Tectonics, 31*, TC4022. https://doi.org/10.1029/2012TC003107

Roskowski, J. A., Patchett, P. J., Spencer, J. E., Pearthree, P. A., Dettman, D. L., Faulds, J. E., & Reynolds, A. C. (2010). A Late Miocene–Early Pliocene chain of lakes fed by the Colorado River: Evidence from Sr, C, and O isotopes of the Bouse Formation and related units between Grand Canyon and the Gulf of California. *Geological Society of America Bulletin, 122*(9–10), 1625–1636. https://doi.org/10.1130/B30186.1

Roy, M., Jordan, T. H., & Pederson, J. L. (2009). Influence of climate change and uplift on Colorado Plateau paleotemperatures from thermochronology. *Tectonics, 28*(5), TC5004. https://doi.org/10.1029/2009TC002449

Sanger, D. (2023). *Magnetostratigraphic constraints of the pre–Colorado River integration Bouse Formation, Blythe Basin, Arizona* (Master's thesis, University of Oklahoma). University of Oklahoma Graduate College.

Schwing, J. (2019). *Magnetostratigraphy of the pre–Colorado River integration Lost Cabin Beds, Cottonwood Valley, Arizona* (Master's thesis, University of Oklahoma). University of Oklahoma Graduate College.

Shoemaker, E. M., Roach, C. H., & Byers, F. M. Jr. (1962). Diatremes and uranium deposits in the Hopi Buttes, Arizona. In *Petrologic Studies—A Volume in Honor of A. F. Buddington* (pp. 327–355). Geological Society of America.

Spencer, J. E., Constenius, K. N., Dettman, D. L., & Domanik, K. J. (2021). Identification of seasonal varves in the lower Pliocene Bouse Formation, lower Colorado River Valley, and implications for Colorado Plateau uplift. *Geosphere, 17*(6), 1745–1761. https://doi.org/10.1130/GES02419.1

Spencer, J. E., Patchett, P. J. (1997). Sr isotope evidence for a lacustrine origin for the upper Miocene to Pliocene Bouse Formation, lower Colorado River trough, and implications for timing of Colorado Plateau uplift. *Geological Society of America Bulletin, 109*(6), 767–778. https://doi.org/10.1130/0016-7606(1997)109<0767:SIEFAL>2.3.CO;2

Spencer, J. E., Pearthree, P. A., House, P. K., Faulds, J. E., & Richard, S. M. (2001). Geologic evolution of the lower Colorado River region. *Arizona Geological Survey Bulletin, 209*, 1–67.

Tanski, N. M., Pederson, J. L., Hidy, A. J., Rittenour, T. M., & Mauch, J. P. (2025). The mystery of baselevel controls in the incision history of the central Colorado Plateau. *AGU Advances, 6*, e2024AV001359. https://doi.org/10.1029/2024AV001359

Thacker, J. O., Karlstrom, K. E., Crossey, L. J., Crow, R. S., Cassidy, C. E., Beard, L. S., ... & Wyatt, M. R. (2020). Post–12 Ma deformation in the lower Colorado River corridor, southwestern USA: Implications for diffuse transtension and the Bouse Formation. *Geosphere*, *16*(1), 111-135.

Van Wijk, J. W., Baldridge, W. S., van Hunen, J., Goes, S., Aster, R., Coblentz, D. D., Grand, S. P., & Ni, J. (2010). Small-scale convection at the edge of the Colorado Plateau: Implications for topography, magmatism, and evolution of Proterozoic lithosphere. *Geology, 38*(7), 611–614. https://doi.org/10.1130/G31031.1

Wernicke, B. (2011). The California River and its role in carving Grand Canyon. *Geological Society of America Bulletin, 123*(7–8), 1288–1316. https://doi.org/10.1130/B30274.1

Winker, C. D., & Kidwell, S. M. (1996). Stratigraphy of a marine rift basin: Neogene of the western Salton Trough, California. In P. L. Abbott & J. D. Cooper (Eds.), *Field Conference Guidebook and Volume for the 1996 Annual Convention of the Pacific Section of the American Association of Petroleum Geologists* (pp. 295–336). Pacific Section AAPG.

Young, R. A., & Spamer, E. E. (Eds.). (2001). *Colorado River: Origin and evolution*. Grand Canyon Association Monograph, 280 p.

Zijderveld, J. D. A. (1967). A.C. demagnetization of rocks: Analysis of results. In D. W. Collinson, K. M. Creer, & S. K. Runcorn (Eds.), *Methods in Palaeomagnetism* (pp. 254–286). Elsevier.